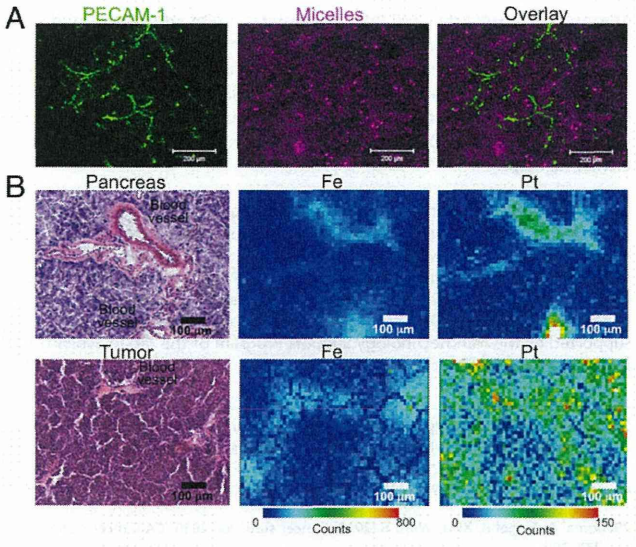

Fig. 6. Microdistribution of DACHPt/m in spontaneous tumors. (*A*) Intratumoral microdistribution of fluorescent-labeled DACHPt/m (magenta) 24 h after administration. Blood vessels were stained with anti-PECAM1 antibody (green). (*B*) Element microdistribution by using μ-SR-XRF in healthy pancreatic tissue (*Upper*) and tumor sections (*Lower*) 24 h after administration of DACHPt/m.

expression of luciferase in the tumors. Moreover, as transgenic tumor models permit studying the cancer development from its earliest steps, for example, histological observations of pancreatic lesions induced by SV40 T have shown areas of dysplastic cells and microadenomas as well as carcinoma (33), they may serve as useful tools for developing nanocarriers capable of targeting early stages of tumor progression for early diagnosis and increased therapeutic efficiency. In this regard, we demonstrated the ability of DACHPt/m to prevent the development of the metastasis, suggesting the potential of the micelles to target early-stage pancreatic cancer. Research in this direction is currently underway in our laboratory.

Our findings strengthen the usefulness of polymeric micelles, particularly of DACHPt/m, for the clinical setting. Delay of disease progression and extension of overall survival time without negatively impacting quality of life may be significant benefits from DACHPt/m.

Materials and Methods

Materials. The chemicals used in this study are listed in *SI Materials and Methods*. EL1-luc/TAg mice were purchased from Caliper Life Science. The production of EL1-luc/TAg mice and the histological features of the tumors have been previously described (30). Mice mating and genotyping details are described in *SI Materials and Methods*. All animal experiments were carried out in accordance with the guidelines for animal experiments at the University of Tokyo, Tokyo.

Synthesis of Block Copolymers. Poly(ethylene glycol)-*b*-poly(L-glutamic acid) [PEG-*b*-P(Glu)] [molecular weight of PEG (MW_{PEG}), 12,000; polymerization degree of P(Glu), 20] was synthesized according to the previously described synthetic method (47). Briefly, *N*-carboxyanhydride of γ-benzyl L-glutamate (BLG-NCA) was synthesized by the Fuchs–Farthing method with triphosgene (48). BLG-NCA was polymerized in dimethylformamide (DMF) initiated by the amino group of CH_3O-PEG-NH_2 to obtain PEG-*b*-poly(γ-benzyl L-glutamate) (PEG-*b*-PBLG). The details regarding the characterization of the block copolymer are described in *SI Materials and Methods*. PEG-*b*-PBLG was deprotected by mixing with 0.5 N NaOH at room temperature to obtain PEG-*b*-P(Glu). Complete deprotection was confirmed by ^{1}H NMR measurement. For the preparation of fluorescent-labeled PEG-*b*-P(Glu), Alexa 647-NHS was mixed with the copolymer in DMSO, dialyzed against water, and purified by column filtration.

Preparation of DACHPt/m. DACHPt/m and Alexa647-DACHPt/m were prepared according to the previously described method (23, 26). DACHPt (5 mM) was suspended in distilled water and mixed with silver nitrate ([$AgNO_3$]/[DACHPt] = 1) to form DACHPt nitrate chloride. The solution was kept in the dark at 25 °C for 24 h. AgCl precipitates were eliminated by centrifugation. The supernatant was purified by passage through a 0.22-μm filter. DACHPt nitrate chloride solution was then mixed with PEG-*b*-P(Glu) ([Glu] = 5 mM; [DACHPt]/[Glu] = 1.0) and reacted for 120 h to obtain DACHPt/m or Alexa647-DACHPt/m, respectively. DACHPt/m and Alexa647-DACHPt/m were purified by ultrafiltration (molecular weight cut-off, 30,000 Da). The platinum content of DACHPt/m was determined by inductively-coupled plasma mass spectrometry (ICP-MS) (4500 ICP-MS; Hewlett Packard).

Isolation of Tumor Cells from EL1-luc/TAg-Induced Acinar Cell Carcinomas and in Vitro Cytotoxicity. Cancer cells were obtained by solid EL1-luc/TAg-induced carcinomas, and the in vitro cytotoxicity against these cells was evaluated. The procedures are described in *SI Materials and Methods*.

In Vivo Antitumor Activity of DACHPt/m. In this experiment, 40 male EL1-luc/TAg mice were used. The experiment started when the mice were at the age of 13 wk. At this time point the tumors were ~3 mm in diameter, matching the observations reported in ref. 30. These tumor regions are highly vascularized with strong bioluminescence signals and histology showing the developed pancreatic carcinoma of acinar cells (30). Moreover, although metastases are not detectable by in vivo bioluminescent imaging at this stage, probably due to their tiny size, Lassota et al. reported the presence of liver metastases by histology (30). Therefore, we considered that the tumors in 13-wk-old mice represent an advanced stage of cancer progression, which is a reasonable approximation of the stage of pancreatic cancer patients commencing chemotherapy (49). Based on the quantification of the bioluminescence signals from the pancreas, the mice were separated into three groups (control, oxaliplatin- and DACHPt/m-treated mice), with the goal to minimize the differences in the mean light emission between these groups. EL1-luc/TAg mice of 13 wk of age were treated over 8 wk with weekly i.v. injection of oxaliplatin (2 and 4 mg/kg) or DACHPt/m (2 mg/kg) on a platinum base. In vivo imaging of luciferase activity in the pancreas was done using an IVIS imaging system (Caliper Life Sciences). Mice were anesthetized with isoflurane and injected i.p. with 150 mg/kg of luciferin. The animals were imaged 10 min after luciferin injection. To reduce variability in measured bioluminescence resulting from variable internal placement of the pancreas, mice were imaged in three positions (ventral, left flank, and right flank). Photons emitted from the pancreas region in each position were quantified using Living Image software, and the sum of these measurements was used as the total bioluminescence signal from the pancreas. Statistical analysis of the bioluminescent signals was performed by Student's *t* test. Moreover, the period when the bioluminescent signal from the tumor remained within 10-fold of the initial value (day 0), without spread of the bioluminescence to the body of the mice, was measured. The threshold at 10-fold of the initial value in bioluminescence was determined in consideration of 2- to 3-fold fluctuation of the signals caused by the quality of i.p. delivery of luciferin, the difference of luciferin distribution kinetics, and the timing of imaging acquisition (30). In addition, the limit of 10-fold increase of the tumor size has been used for indicating the growth delay of the disease by different therapeutic approaches (50, 51). The overall survival was directly measured by counting deceased animals. The statistical analysis of the 10-fold increase of bioluminescence and overall survival was calculated using the log-rank test (Mantel–Cox) using GraphPad Prism software (GraphPad).

The CA19-9 expression was also studied to determine the tumor extent as described in *SI Materials and Methods*.

Drug Accumulation in Pancreas and Tumors. Biodistribution studies were carried out on EL1-luc/TAg mice and wild-type mice (18 wk of age). Oxaliplatin (5 mg/kg) and DACHPt/m (5 mg/kg) were i.v. injected into mice. The mice were killed after 24 h. Whole pancreases, including tumor tissue and normal pancreatic tissue for EL1-luc/TAg mice, were excised. The samples were dissolved in HNO_3 and evaporated to dryness. The Pt concentrations were then measured by ICP-MS. Statistical analysis was performed by Student's *t* test.

Histology and Immunohistochemistry. Alexa 647-DACHPt/m (10 mg/kg) was administered i.v. into EL1-luc/TAg mice of 18 wk of age. Mice were killed at 24 h postinjection. The excised samples were directly frozen in liquid N_2 for immunohistochemistry or fixed in 4% (vol/vol) paraformaldehyde and then embedded in paraffin to prepare the tissue sections for H&E staining. For immunohistochemical staining, frozen samples were sectioned at 10-μm thickness in a cryostat, fixed in acetone, and incubated with protein blocking solution (Blocking One Buffer, Nakalai Tesque). The sections

were reacted with antimurine PECAM1 monoclonal antibody (Mec13.3; BD Pharmingen; 553370), rabbit polyclonal antibody against PDGFRβ (Upstate Group; 06–498),and monoclonal anti–α-SMA antibody (Sigma-Aldrich; A2547). Samples were subsequently stained with secondary antibodies conjugated with Alexa Fluor 488, 594, or 647 anti-rat/rabbit IgG (Invitrogen Molecular Probes). The samples were observed by using an Olympus AX80 microscope for H&E staining and a Zeiss LSM510 Meta confocal microscope for immunohistochemistry.

Microsynchrotron Radiation X-Ray Fluorescence Spectrometry Analysis. EL1-luc/TAg mice of 18 wk of age were injected i.v. with doses of 20 mg/kg (on a Pt base) of DACHPt/m. Twenty-four hours after the injection, the mice were killed and the tumors were excised, embedded in Tissue-Tek optimal cutting temperature compound (Sakura Finetek) and kept at −80 °C. These samples were sliced at 20 μm using a cryostat and fixed on a polypropylene sheet. μ-SR-XRF was performed using beamline 37XU (52) at SPring-8, operated at 8 GeV and ∼100 mA. The tissue samples were irradiated with incident X-rays with an energy of 14 keV, a beam spot size of $1.3 \times 1.3\ \mu m^2$, and an intensity of 10^{12} photons per second. The fluorescence X-rays were measured using a Si solid-state detector in air at room temperature. Each sample was mounted on an *x–y* translation stage. The fluorescence X-ray intensity was normalized by the incident X-ray intensity, I_0, to produce a 2D elemental map.

ACKNOWLEDGMENTS. The authors thank S. Ogura and K. Date for assistance with animal care. This research was supported by the Funding Program for World-Leading Innovative Research and Development on Science and Technology (FIRST Program) from the Japan Society for the Promotion of Science and Grants-in-Aid for Scientific Research from the Japanese Ministry of Health, Labour, and Welfare. μ-Synchroton radiation–X-ray fluorescence studies were supported by the Nanotechnology Support Program of the Japan Synchrotron Radiation Research Institute.

1. Heidel JD, Davis ME (2011) Clinical developments in nanotechnology for cancer therapy. *Pharm Res* 28(2):187–199.
2. Peer D, et al. (2007) Nanocarriers as an emerging platform for cancer therapy. *Nat Nanotechnol* 2(12):751–760.
3. Duncan R (2006) Polymer conjugates as anticancer nanomedicines. *Nat Rev Cancer* 6(9):688–701.
4. Miyata K, Christie RJ, Kataoka K (2011) Polymeric micelles for nano-scale drug delivery. *React Funct Polym* 7(3):227–234.
5. Matsumura Y, Maeda H (1986) A new concept for macromolecular therapeutics in cancer chemotherapy: Mechanism of tumoritropic accumulation of proteins and the antitumor agent smancs. *Cancer Res* 46(12 Pt 1):6387–6392.
6. Frese KK, Tuveson DA (2007) Maximizing mouse cancer models. *Nat Rev Cancer* 7(9): 645–658.
7. Politi K, Pao W (2011) How genetically engineered mouse tumor models provide insights into human cancers. *J Clin Oncol* 29(16):2273–2281.
8. Johnson JI, et al. (2001) Relationships between drug activity in NCI preclinical in vitro and in vivo models and early clinical trials. *Br J Cancer* 84(10):1424–1431.
9. Voskoglou-Nomikos T, Pater JL, Seymour L (2003) Clinical predictive value of the in vitro cell line, human xenograft, and mouse allograft preclinical cancer models. *Clin Cancer Res* 9(11):4227–4239.
10. Sacco MG, et al. (2000) Liposome-delivered angiostatin strongly inhibits tumor growth and metastatization in a transgenic model of spontaneous breast cancer. *Cancer Res* 60(10):2660–2665.
11. Hamzah J, et al. (2009) Targeted liposomal delivery of TLR9 ligands activates spontaneous antitumor immunity in an autochthonous cancer model. *J Immunol* 183(2): 1091–1098.
12. Wicki A, et al. (2012) Targeting tumor-associated endothelial cells: Anti-VEGFR2 immunoliposomes mediate tumor vessel disruption and inhibit tumor growth. *Clin Cancer Res* 18(2):454–464.
13. Sengupta P, et al. (2012) Cholesterol-tethered platinum II-based supramolecular nanoparticle increases antitumor efficacy and reduces nephrotoxicity. *Proc Natl Acad Sci USA* 109(28):11294–11299.
14. Huang Y-H, et al. (2009) Nanoparticle-delivered suicide gene therapy effectively reduces ovarian tumor burden in mice. *Cancer Res* 69(15):6184–6191.
15. Tanaka E, Choi HS, Fujii H, Bawendi MG, Frangioni JV (2006) Image-guided oncologic surgery using invisible light: Completed pre-clinical development for sentinel lymph node mapping. *Ann Surg Oncol* 13(12):1671–1681.
16. Veiseh O, et al. (2009) Specific targeting of brain tumors with an optical/magnetic resonance imaging nanoprobe across the blood-brain barrier. *Cancer Res* 69(15): 6200–6207.
17. Olson ES, et al. (2010) Activatable cell penetrating peptides linked to nanoparticles as dual probes for in vivo fluorescence and MR imaging of proteases. *Proc Natl Acad Sci USA* 107(9):4311–4316.
18. Daldrup-Link HE, et al. (2011) MRI of tumor-associated macrophages with clinically applicable iron oxide nanoparticles. *Clin Cancer Res* 17(17):5695–5704.
19. Mikhaylov G, et al. (2011) Ferri-liposomes as an MRI-visible drug-delivery system for targeting tumours and their microenvironment. *Nat Nanotechnol* 6(9):594–602.
20. Nishiyama N, Kataoka K (2006) Current state, achievements, and future prospects of polymeric micelles as nanocarriers for drug and gene delivery. *Pharmacol Ther* 112(3): 630–648.
21. Matsumura Y, Kataoka K (2009) Preclinical and clinical studies of anticancer agent-incorporating polymer micelles. *Cancer Sci* 100(4):572–579.
22. Plummer R, et al. (2011) A Phase I clinical study of cisplatin-incorporated polymeric micelles (NC-6004) in patients with solid tumours. *Br J Cancer* 104(4):593–598.
23. Cabral H, Nishiyama N, Okazaki S, Koyama H, Kataoka K (2005) Preparation and biological properties of dichloro(1,2-diaminocyclohexane)platinum(II) (DACHPt)-loaded polymeric micelles. *J Control Release* 101(1-3):223–232.
24. Cabral H, Nishiyama N, Kataoka K (2007) Optimization of (1,2-diamino-cyclohexane) platinum(II)-loaded polymeric micelles directed to improved tumor targeting and enhanced antitumor activity. *J Control Release* 121(3):146–155.
25. Murakami M, et al. (2011) Improving drug potency and efficacy by nanocarrier-mediated subcellular targeting. *Sci Transl Med* 3(64):64ra2.
26. Cabral H, et al. (2011) Accumulation of sub-100 nm polymeric micelles in poorly permeable tumours depends on size. *Nat Nanotechnol* 6(12):815–823.
27. Rafi M, et al. (2012) Polymeric micelles incorporating (1,2-diaminocyclohexane)platinum (II) suppress the growth of orthotopic scirrhous gastric tumors and their lymph node metastasis. *J Control Release* 159(2):189–196.
28. American Cancer Society (2011) *Cancer Facts & Figures 2011* (American Cancer Society, Atlanta).
29. Jemal A, Siegel R, Xu J, Ward E (2010) Cancer statistics, 2010. *CA Cancer J Clin* 60(5): 277–300.
30. Zhang N, Lyons S, Lim E, Lassota P (2009) A spontaneous acinar cell carcinoma model for monitoring progression of pancreatic lesions and response to treatment through noninvasive bioluminescence imaging. *Clin Cancer Res* 15(15):4915–4924.
31. Ornitz DM, Hammer RE, Messing A, Palmiter RD, Brinster RL (1987) Pancreatic neoplasia induced by SV40 T-antigen expression in acinar cells of transgenic mice. *Science* 238(4824):188–193.
32. Longnecker DS, Kuhlmann ET, Freeman DH, Jr. (1990) Characterization of the elastase 1-simian virus 40 T-antigen mouse model of pancreatic carcinoma: Effects of sex and diet. *Cancer Res* 50(23):7552–7554.
33. Tevethia MJ, Bonneau RH, Griffith JW, Mylin L (1997) A simian virus 40 large T-antigen segment containing amino acids 1 to 127 and expressed under the control of the rat elastase-1 promoter produces pancreatic acinar carcinomas in transgenic mice. *J Virol* 71(11):8157–8166.
34. Graham MA, et al. (2000) Clinical pharmacokinetics of oxaliplatin: A critical review. *Clin Cancer Res* 6(4):1205–1218.
35. Pasetto LM, D'Andrea MR, Rossi E, Monfardini S (2006) Oxaliplatin-related neurotoxicity: How and why? *Crit Rev Oncol Hematol* 59(2):159–168.
36. Ling B, Authier N, Balayssac D, Eschalier A, Coudore F (2007) Behavioral and pharmacological description of oxaliplatin-induced painful neuropathy in rat. *Pain* 128(3): 225–234.
37. Duffy MJ, et al. (2010) Tumor markers in pancreatic cancer: A European Group on Tumor Markers (EGTM) status report. *Ann Oncol* 21(3):441–447.
38. Esteban-Fernández D, Verdaguer JM, Ramírez-Camacho R, Palacios MA, Gómez-Gómez MM (2008) Accumulation, fractionation, and analysis of platinum in toxicologically affected tissues after cisplatin, oxaliplatin, and carboplatin administration. *J Anal Toxicol* 32(2):140–146.
39. Vignot S, Faivre S, Aguirre D, Raymond E (2005) mTOR-targeted therapy of cancer with rapamycin derivatives. *Ann Oncol* 16(4):525–537.
40. Kano MR, et al. (2007) Improvement of cancer-targeting therapy, using nanocarriers for intractable solid tumors by inhibition of TGF-β signaling. *Proc Natl Acad Sci USA* 104(9):3460–3465.
41. Zhang L, Nishihara H, Kano MR (2012) Pericyte-coverage of human tumor vasculature and nanoparticle permeability. *Biol Pharm Bull* 35(5):761–766.
42. Trédan O, Galmarini CM, Patel K, Tannock IF (2007) Drug resistance and the solid tumor microenvironment. *J Natl Cancer Inst* 99(19):1441–1454.
43. Minchinton AI, Tannock IF (2006) Drug penetration in solid tumours. *Nat Rev Cancer* 6(8):583–592.
44. Yasunaga M, Manabe S, Matsumura Y (2011) New concept of cytotoxic immunoconjugate therapy targeting cancer-induced fibrin clots. *Cancer Sci* 102(7):1396–1402.
45. Nishida K, Yonemura K, Abe Y, Takagi K (1995) Antitumor effects of liposomes containing adriamycin on chemically-induced rat malignant fibrous histiocytoma. *Nippon Seikeigeka Gakkai Zasshi* 69(5):322–331.
46. Yazawa K, et al. (2001) Bifidobacterium longum as a delivery system for gene therapy of chemically induced rat mammary tumors. *Breast Cancer Res Treat* 66(2):165–170.
47. Nishiyama N, et al. (2003) Novel cisplatin-incorporated polymeric micelles can eradicate solid tumors in mice. *Cancer Res* 63(24):8977–8983.
48. Daly WH, Poche D (1988) The preparation of N-carboxyanhydrides of a-amino acids using bis(trichloromethyl)carbonate. *Tetrahedron Lett* 29(46):5859–5862.
49. Heinemann V, Haas M, Boeck S (2012) Systemic treatment of advanced pancreatic cancer. *Cancer Treat Rev* 38(7):843–853.
50. Schlom J, et al. (1992) Therapeutic advantage of high-affinity anticarcinoma radioimmunoconjugates. *Cancer Res* 52(5):1067–1072.
51. Cao C, et al. (2006) Vascular endothelial growth factor tyrosine kinase inhibitor AZD2171 and fractionated radiotherapy in mouse models of lung cancer. *Cancer Res* 66(23):11409–11415.
52. Terada Y, et al. (2004) Construction and commissioning of BL37XU at SPring-8. *AIP Conf Proc* 705(1):376–379.

siRNA Conjugates

DOI: 10.1002/anie.201300178

Acidic pH-Responsive siRNA Conjugate for Reversible Carrier Stability and Accelerated Endosomal Escape with Reduced IFNα-Associated Immune Response**

Hiroyasu Takemoto, Kanjiro Miyata, Shota Hattori, Takehiko Ishii, Tomoya Suma, Satoshi Uchida, Nobuhiro Nishiyama, and Kazunori Kataoka**

Small interfering RNA (siRNA) has garnered much interest as a potential drug because of its strong gene-silencing activity.[1] Toward the success in siRNA therapeutics, many strategies have been developed for efficient siRNA delivery into the cytosol of target cells.[2] Among them, siRNA conjugates have arisen as one of the promising strategies in siRNA delivery, as siRNA can be readily conjugated to a functional molecule to acquire the ability of "programmed transfer" to the target sites.[3] Indeed, several ligand molecules, such as lactose and RGD peptide, were conjugated with siRNA for site- (or cell)-specific delivery.[3] Furthermore, multimolecular siRNA conjugates enable stable polyion complex (PIC) formation because of the increased electrostatic interactions with polycations, leading to facilitated cellular uptake through charge neutralization of siRNA and also protection of siRNA from enzymatic degradations.[4] However, those siRNA conjugates potentially stimulate immune responses through the activation of toll-like receptor 3 and/or protein kinase R,[4,5] and thus they are desired to disintegrate into monomeric siRNAs (mono-siRNAs) in the cell for reduced immune responses.[4] Meanwhile, considering that macromolecular drugs, including siRNA and its conjugates, would be taken up by cells through endocytosis and then delivered to the late endosome toward lysosomal degradation, siRNA needs to escape from the endosome into the cytosol for efficient gene silencing.[6] Therefore, design of a smart siRNA conjugate for programmed endosomal escape and release of mono-siRNA is a great challenge for successful siRNA delivery.

Herein, we developed a smart siRNA conjugate to fulfill the multifunctionality desired for enhanced siRNA delivery with reduced immunogenicity; that is, reversible PIC stability, endosomal escapability, and mono-siRNA releasability, based on a single chemical process. It is known that maleic acid amide (MAA) is relatively stable at extracellular neutral pH, while rapidly hydrolyzed at endosomal acidic pH.[7] Thus, we utilized this MAA chemistry as an acid-labile anionic moiety for linking siRNA to an endosome-disrupting polycation and concurrently converting the cationic sites into a biologically inert anionic derivative.[8] In design, the MAA-based conjugate is expected to improve the PIC stability through increased electrostatic interaction, while degrading the MAA moieties in the endosome for triggering three actions: 1) complex destabilization through unbalanced charges within PICs; 2) endosome disruption with the regenerated parent polycation; and 3) mono-siRNA release by MAA cleavage (Figure 1a). Figure 1b shows the chemical structure of siRNA-releasable/endosome-disrupting conjugate (REC), in which several siRNA molecules are grafted into the endosome-disrupting polymer side chains by the MAA linkage. The parent polycation is a polyaspartamide derivative with two repeating units of aminoethylene in each side chain (termed PAsp(DET)), which destabilizes the endosomal membrane integrity with the cationic diprotonated side chains to accelerate endosomal escape of the payload.[9]

A precursor polyanion was synthesized from PAsp(DET) to have a dibenzyl cyclooctyne (DBCO) group by MAA linkage as a conjugation site for siRNA. Then, an azide-modified siRNA (azide-siRNA) was reacted with the DBCO group in the polyanion side chains. Notably, the size exclusion chromatography (Supporting Information, Figure S5) confirmed that more than 95% of azide-siRNAs were conjugated to the polymer backbone utilizing a freeze–thaw treatment for the generation of a highly concentrated reactant phase.[10] This successful conjugation at the quite high rate allows the use of the obtained conjugate without further purification. As a result, about 30% of DBCO groups in the polymer side chains reacted with azide-siRNA; that is, about 5 siRNAs contained in the conjugate (Figure 1b). To investigate the

[*] H. Takemoto, Dr. K. Kataoka
Department of Materials Engineering, The University of Tokyo
Hongo 7-3-1, Bunkyo-ku, Tokyo 113-8656 (Japan)
E-mail: kataoka@bmw.t.u-tokyo.ac.jp
Homepage: http://www.bmw.t.u-tokyo.ac.jp/
S. Hattori, Dr. T. Ishii, T. Suma
Department of Bioengineering, The University of Tokyo
Hongo 7-3-1, Bunkyo-ku, Tokyo 113-8656 (Japan)
Dr. K. Miyata, S. Uchida
Division of Clinical Biotechnology, Center for Disease Biology and Integrative Medicine, The University of Tokyo
Hongo 7-3-1, Bunkyo-ku, Tokyo 113-0033 (Japan)
E-mail: miyata@bmw.t.u-tokyo.ac.jp
Dr. N. Nishiyama
Polymer Chemistry Division, Chemical Resources Laboratory
Tokyo Institute of Technology, R1-11
4259 Nagatsuta, Midori-ku, Yokohama 226-8503 (Japan)

[**] This research is supported by the Japan Society for the Promotion of Science (JSPS) through the "Funding Program for World-Leading Innovative R&D on Science and Technology (FIRST Program)," and Health and Labour Sciences Research Grants Research on Medical Device Development, Ministry of Health, Labour and Welfare. H.T. thanks the Research Fellowships of the Japan Society for the Promotion of Science for Young Scientists (JSPS).

Supporting information for this article is available on the WWW under http://dx.doi.org/10.1002/anie.201300178.

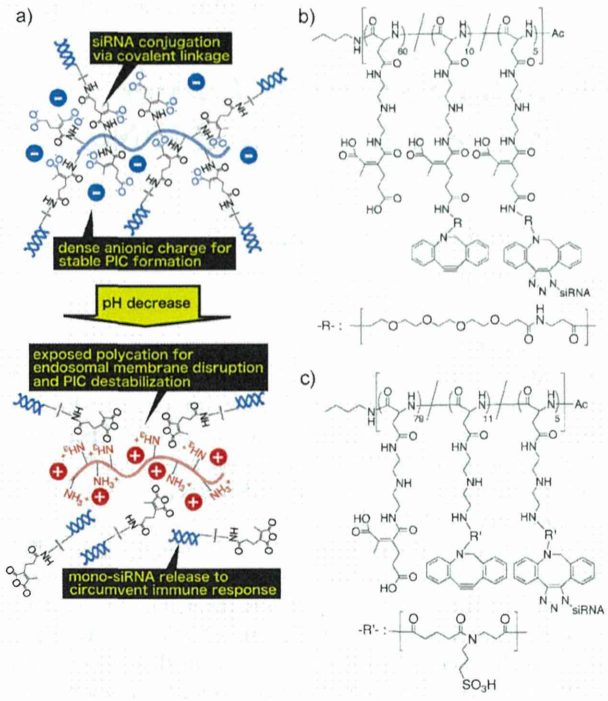

Figure 1. a) Illustration of releasable/enzyme-disrupting conjugate (REC) with the multifunctionality toward endosomal escape and release of mono-siRNA. b) Chemical structure of REC. c) Chemical structure of uREC. The PAsp derivative in this study has the mixed sequence of α and β isomers. Only α isomers are depicted in (b) and (c) for simplicity.

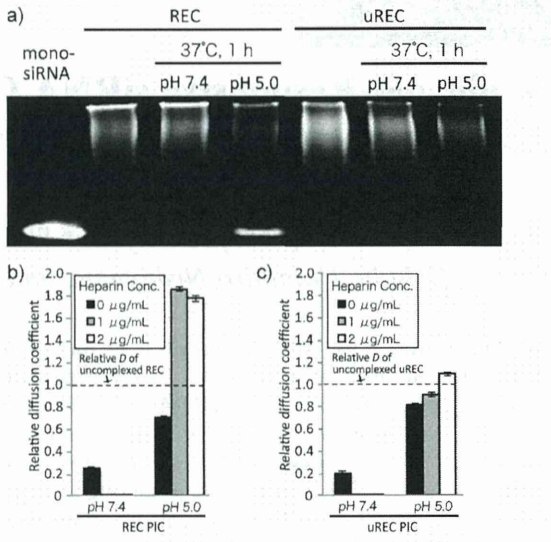

Figure 2. a) PAGE analysis of REC and uREC before and after 1 h incubation at 37 °C and at pH 7.4 or pH 5.0. b),c) Relative *D* values of siRNA conjugate PICs after a 30 min incubation at 37 °C with various heparin concentrations at pH 7.4 or pH 5.0. Relative *D* values are calculated by normalization of *D* to that of uncomplexed siRNA conjugates; REC PIC (b) and uREC PIC (c). Results were shown as mean and standard deviation obtained from 10 measurements.

effect of MAA linkage on the siRNA releasability, another siRNA conjugate, in which the DBCO group was directly conjugated to primary amines in PAsp(DET) without MAA linkage, was also synthesized as an siRNA-unreleasable but endosome-disrupting control (uREC; Figure 1c). The obtained siRNA conjugates were analyzed for their pH-sensitivity by polyacrylamide gel electrophoresis (PAGE) analysis (Figure 2a). The retarded bands in siRNA conjugates, compared to mono-siRNA, indicate that both siRNA conjugates had significantly higher molecular weight than mono-siRNA. A 1 h incubation of REC at pH 5.0 resulted in the band appearance at the same position as mono-siRNA, whereas such band was not observed at pH 7.4, indicating that mono-siRNA release was triggered selectively at the acidic pH. In contrast, the band corresponding to mono-siRNA was not observed for uREC after a 1 h incubation at both pHs of 5.0 and 7.4, indicating the essential role of MAA linkage for mono-siRNA release from REC.

Next, siRNA conjugates were mixed with a polycation PAsp(DET) to form PICs at N/P 10 (residual molar ratio of amines of PAsp(DET) to phosphates of siRNA) for their facilitated cellular uptake. PIC formation with siRNA conjugates as well as mono-siRNA was confirmed by fluorescence correlation spectroscopy (FCS) using Cy3-labeled siRNA (Cy3-siRNA) and its conjugates (Supporting Information, Table S2) as well as agarose gel electrophoresis (Supporting Information, Figure S6). The diffusion coefficients *D* in 10 mM HEPES buffer (pH 7.4) were determined to be 66.2 $\mu m^2 s^{-1}$ for mono-siRNA PIC and 2.9 $\mu m^2 s^{-1}$ for both siRNA conjugate PICs. These values were significantly smaller than those of the uncomplexed controls; that is, mono-siRNA (94.5 $\mu m^2 s^{-1}$) and siRNA conjugates (15.5 $\mu m^2 s^{-1}$ for REC and 18.8 $\mu m^2 s^{-1}$ for uREC). Considering that the *D* value of nanoparticles is inversely correlated with their size,[11] the smaller *D* values in the presence of polycation indicate successful PIC formation with the siRNA conjugates as well as mono-siRNA in the aqueous condition (siRNA concentration: 100 nM). The substantially smaller *D* values of the conjugate PICs, compared to the mono-siRNA PIC, indicate a larger association number of siRNA in the conjugate PICs, which is presumably due to increased anionic charges in the conjugate. Then, the acidic pH-sensitive PIC stability was further evaluated by FCS after a 30 min incubation of PICs at 37 °C in 10 mM HEPES (pH 7.4) and 10 mM MES (pH 5.0) containing heparin. Heparin is a major component of extracellular matrices on cellular surface and probably serves as a strong polyanionic counterpart to induce PIC dissociation.[12] The obtained *D* values of each sample were normalized to that of the corresponding uncomplexed siRNA control; that is, uncomplexed REC for REC PIC, uncomplexed uREC for uREC PIC, and uncomplexed mono-siRNA for mono-siRNA PIC (Figure 2b,c; Supporting Information, Figure S7, respectively). After incubation with heparin, a relative *D* of mono-siRNA PICs progressively increased with the increase in heparin concentration similarly at both pH values of 7.4 and 5.0, indicating that mono-siRNA PICs gradually dissociated with the increased counter polyanion, regardless of the environmental pH (Supporting Information, Figure S7). In contrast, relative *D* values of

REC and uREC PICs decreased after incubation with heparin at pH 7.4, suggesting that the conjugated siRNA is more stably encapsulated within PICs, compared to mono-siRNA, even after binding of heparin onto PIC surface. Notably, the incubation of REC and uREC PICs at pH 5.0 dramatically increased their relative *D* values, and furthermore, the increase in the relative *D* values was facilitated in the presence of heparin, indicating the acidic pH-responsive destabilization of the siRNA conjugate PICs (Figure 2b,c). Considering the fact that the MAA linkage contained in both siRNA conjugates can degrade at pH 5.0 to generate the polycations in PIC, the destabilization of siRNA conjugate PICs at pH 5.0 is presumably due to the electrostatic repulsion between the generated polycations and the originally incorporated polycations in PIC. Furthermore, the increased relative *D* values of REC PICs in the presence of heparin, beyond that of uncomplexed REC, strongly suggest the mono-siRNA release triggered by the cleavage of MAA linkage. These results demonstrate that the acidic pH-sensitivity of the MAA-based conjugates can be maintained even after PIC formation, and also they provide siRNA PICs with a reversible stability in response to the intracellular environment.

Delivery functionalities of REC PICs, namely cellular uptake efficiency and intracellular trafficking profile, were evaluated with cultured human ovarian cancer cells stably expressing luciferase (SKOV3-Luc). Cellular uptake of siRNA was estimated using Cy3-siRNA with a fluorescence microscopy (Supporting Information, Figure S8). REC and uREC PICs (N/P 10) allowed 30% increase in Cy3 fluorescence from cells compared to mono-siRNA PICs (N/P 10, $p < 0.005$), indicating that the conjugate formulation significantly enhanced the cellular uptake of siRNA is probably due to the higher stability, as suggested by the FCS result at pH 7.4 (Figure 2b,c; Supporting Information, Figure S7). Next, confocal laser scanning microscopic (CLSM) observation was performed to examine subcellular distribution of siRNA PICs (N/P 10), especially focusing on the colocalization of siRNA with the late endosome/lysosome as an indicator for endosomal entrapment (Figure 3a–c).[13] In the cells treated with mono-siRNA PICs, the colocalization (yellow) ratio of Cy3-siRNA (red) with a late endosome/lysosome marker LysoSensor Green (green) was increased up to 70% for the initial 12 h and then kept constant for subsequent 36 h (Figure 3d). In contrast, the cells treated with REC and uREC PICs showed that the colocalization ratio was progressively decreased over incubation period and reached about 30% after a 48 h incubation. The significantly lower colocalization ratios (or less endosomal entrapment) of REC/uREC PICs strongly suggest more efficient endosomal escape of siRNA compared to mono-siRNA PICs (Figure 3d). This enhanced endosomal escape with REC and uREC is consistent with the endosome-disrupting functionality of the backbone polymer, which should be converted into the parent polycation PAsp(DET) in the acidic late endosome/lysosome for the membrane disruption, as suggested by a membrane disruption assay at pH 7.4 and 5.0 (Supporting Information, Figure S9).[8,9]

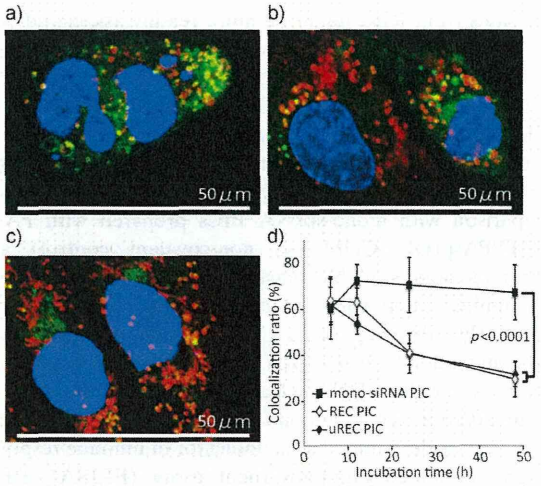

Figure 3. a–c) CLSM images 48 h after treatment of SKOV3-Luc cells with mono-siRNA PIC (a), REC PIC (b), and uREC PIC (c). Red Cy3-siRNA, green late endosome/lysosome (LysoSensor Green), blue nucleus (Hoechst 33342). A yellow pixel indicates colocalization between a red pixel and green pixel. d) Time-dependent change in the colocalization ratio between Cy3-siRNA and late endosome/lysosome. The colocalization ratio was shown as mean and standard deviation obtained from 10 cells. The *p* value was calculated according to Student's *t* test.

Next, the gene silencing ability of REC PICs was compared with mono-siRNA and uREC PICs by luciferase assay with cultured SKOV3-Luc cells (Figure 4a). Obviously, REC and uREC PICs achieved more efficient sequence-specific gene silencing in the cells than mono-siRNA PICs, which is presumably due to the enhanced endosomal escape of siRNA conjugate PICs (Figure 3) as well as facilitated cellular uptake of siRNA (Supporting Information, Figure S8). Interestingly, REC PICs induced significantly stronger gene silencing than uREC PICs ($p < 0.005$), demonstrating the positive effect of siRNA releasability by the MAA linkage on the siRNA delivery functionality. Mono-siRNA

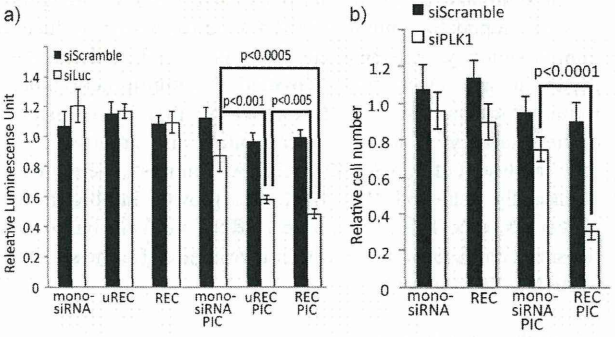

Figure 4. a) Luciferase gene expression in cultured SKOV3-Luc cells after PIC treatment at 100 nM Luc siRNA (siLuc) or scramble siRNA (siScramble) for 48 h. b) Cell viability in cultured A549 cells after PIC treatment at 100 nM PLK1 siRNA (siPLK1) or siScramble for 72 h. In both figures, results were shown as mean and standard deviation obtained from 6 samples. The *p* values were calculated according to Student's *t* test.

releasates from REC might be more readily associated with the gene silencing pathway owing to compromised steric hindrance compared to the conjugated structure. Also, no cytotoxicity was observed for all the tested PIC formulations under the same conditions as the gene-silencing assay (Supporting Information, Figure S10). Significantly stronger luciferase gene silencing of REC PICs was also confirmed in comparison with mono-siRNA PICs prepared with PAsp-(DET)/PAsp(DET-CDM) (a non-covalent control) and a commercially available reagent ExGen500 (linear polyethylenimine; Supporting Information, Figure S11), demonstrating the advantage of REC formulation, including covalent conjugation between siRNA and the backbone polymer. The effect of the siRNA-releasability of REC was further examined from the standpoint of immune responses; IFNα response was determined as an indicator of immune response by enzyme-linked immunosorbent assay (ELISA). REC, uREC, and their PICs did not induce a detectable level of IFNα production for SKOV3-Luc cells ($< 10\ pg\,mL^{-1}$, data not shown). Thus, the similar ELISA experiment was further challenged for murine macrophage cells (Raw264.7), which are known to be highly sensitive to immunogen.[14] As a result, REC PICs induced a significantly lower level of IFNα production ($24.3 \pm 3.5\ pg\,mL^{-1}$) compared to uREC PICs ($60.8 \pm 12.9\ pg\,mL^{-1}$, $p < 0.005$), indicating that the siRNA-releasability based on MAA linkage successfully decreased the immune response for siRNA conjugates. Uncomplexed REC and uREC without polycation did not induce a detectable level of IFNα production, suggesting that they should not stimulate IFNα response at least on the cellular surface. Finally, the utility of REC PICs was verified for other cell lines, using a therapeutic siRNA targeting polo-like kinase 1 (PLK1). PLK1 is known to be a cell cycle regulator, and thus its silencing can arrest the cell cycle toward the apoptosis.[15] REC PICs with PLK1 siRNA (N/P 20) sequence-specifically suppressed the growth of human lung carcinoma cells (A549) and human hepatocarcinoma cells (Huh-7; Figure 4b; Supporting Information, Figure S12, respectively), demonstrating a strong potential of the REC formulation bearing the MAA linkage for siRNA-based cancer therapy.

In summary, an acidic pH-responsive siRNA conjugate was developed for enhanced siRNA delivery with reduced immunogenicity. A single chemical process based on the MAA linkage successfully provided the multifunctionality required for successful siRNA delivery; that is, reversible carrier stability, endosomal escapability, and mono-siRNA releasability. Ultimately, the siRNA conjugate sequence-specifically achieved the significant growth inhibition of cancerous cells. The programmed siRNA delivery based on the smart conjugate will be further investigated for the success in siRNA therapeutics.

Received: January 9, 2013
Revised: February 25, 2013
Published online: April 29, 2013

Keywords: conjugation · drug delivery · drug design · polymers · siRNA

[1] a) S. M. Elbashir, J. Harborth, W. Lendeckel, A. Yalcin, K. Weber, T. Tuschl, *Nature* **2001**, *411*, 494–498; b) J. C. Burnett, J. J. Rossi, *Chem. Biol.* **2012**, *19*, 60–71.

[2] R. L. Kanasty, K. A. Whitehead, A. J. Vegas, D. G. Anderson, *Mol. Ther.* **2012**, *20*, 513–524.

[3] a) D. B. Rozema, D. L. Lewis, D. H. Wakefield, S. C. Wong, J. J. Klein, P. L. Roesch, S. L. Bertin, T. W. Reppen, Q. Chu, A. V. Blokhin, J. E. Hagstrom, J. A. Wolf, *Proc. Natl. Acad. Sci. USA* **2007**, *104*, 12982–12987; b) Y. Singh, P. Murat, E. Defrancq, *Chem. Soc. Rev.* **2010**, *39*, 2054–2070; c) M. R. Alam, X. Ming, M. Fisher, J. G. Lackey, K. G. Rajeev, M. Manoharan, R. L. Juliano, *Bioconjugate Chem.* **2011**, *22*, 1673–1681; d) S. K. Lee, A. Siefert, J. Beloor, T. M. Fahmy, P. Kumar, *Methods Enzymol.* **2012**, *502*, 91–122.

[4] a) A.-L. Bolcato-Bellemin, M.-E. Bonnet, G. Creusat, P. Erbacher, J.-P. Behr, *Proc. Natl. Acad. Sci. USA* **2007**, *104*, 16050–16055; b) H. Mok, S. H. Lee, J. W. Park, T. G. Park, *Nat. Mater.* **2010**, *9*, 272–278; c) H. Takemoto, A. Ishii, K. Miyata, M. Nakanishi, M. Oba, T. Ishii, Y. Yamasaki, N. Nishiyama, K. Kataoka, *Biomaterials* **2010**, *31*, 8097–8105; d) C. A. Hong, S. H. Lee, J. S. Kim, J. W. Park, K. H. Bae, H. Mok, T. G. Park, H. Lee, *J. Am. Chem. Soc.* **2011**, *133*, 13914–13917; e) S. J. Lee, M. S. Huh, S. Y. Lee, S. Min, S. Lee, H. Koo, J. U. Chu, K. E. Lee, H. Jeon, Y. Choi, K. Choi, Y. Byun, S. Y. Jeong, K. Park, K. Kim, I. C. Kwon, *Angew. Chem.* **2012**, *124*, 7315–7319; *Angew. Chem. Int. Ed.* **2012**, *51*, 7203–7207.

[5] A. Judge, I. MacLachlan, *Hum. Gene Ther.* **2008**, *19*, 111–124.

[6] a) C. Troiber, E. Wagner, *Bioconjugate Chem.* **2011**, *22*, 1737–1752; b) J. Nguyen, F. C. Szoka, *Acc. Chem. Res.* **2012**, *45*, 1153–1162.

[7] a) D. B. Rozema, K. Ekena, D. L. Lewis, A. G. Loomis, J. A. Wolff, *Bioconjugate Chem.* **2003**, *14*, 51–57; b) S. Guo, Y. Huang, Q. Jiang, Y. Sun, L. Deng, Z. Liang, Q. Du, J. Xing, Y. Zhao, P. C. Wang, A. Dong, X.-J. Liang, *ACS Nano* **2010**, *4*, 5505–5511.

[8] Y. Lee, K. Miyata, M. Oba, T. Ishii, S. Fukushima, M. Han, H. Koyama, N. Nishiyama, K. Kataoka, *Angew. Chem.* **2008**, *120*, 5241–5244; *Angew. Chem. Int. Ed.* **2008**, *47*, 5163–5166.

[9] K. Miyata, M. Oba, M. Nakanishi, S. Fukushima, Y. Yamasaki, H. Koyama, N. Nishiyama, K. Kataoka, *J. Am. Chem. Soc.* **2008**, *130*, 16287–16294.

[10] H. Takemoto, K. Miyata, T. Ishii, S. Hattori, S. Osawa, N. Nishiyama, K. Kataoka, *Bioconjugate Chem.* **2012**, *23*, 1503–1506.

[11] J. DeRouchey, C. Schmidt, G. F. Walker, C. Koch, C. Plank, E. Wagner, J. O. Radler, *Biomacromolecules* **2008**, *9*, 724–732.

[12] a) M. J. Palte, R. T. Raines, *J. Am. Chem. Soc.* **2012**, *134*, 6218–6223; b) M. Zheng, D. Librizzi, A. Kılıç, Y. Liu, H. Renz, O. M. Merkel, T. Kissel, *Biomaterials* **2012**, *33*, 6551–6558.

[13] K. Whitehead, G. Sahay, G. Z. Li, K. T. Love, C. A. Alabi, M. Ma, C. Zurenko, W. Querbes, R. S. Langer, D. G. Anderson, *Mol. Ther.* **2011**, *19*, 1688–1694.

[14] J. Turco, H. H. Winker, *Infect. Immun.* **1982**, *35*, 783–791.

[15] a) A. D. Judge, M. Robbins, I. Tavakoli, J. Levi, L. Hu, A. Fronda, E. Ambegia, K. McClintock, I. MacLachlan, *J. Clin. Invest.* **2009**, *119*, 661–673; b) K. Strebhardt, *Nat. Rev. Drug Discovery* **2010**, *9*, 643–660.

Virchows Arch (2015) 466:265–277
DOI 10.1007/s00428-014-1705-4

ORIGINAL ARTICLE

An immunohistochemical marker panel including claudin-18, maspin, and p53 improves diagnostic accuracy of bile duct neoplasms in surgical and presurgical biopsy specimens

Yoshiko Keira · Akira Takasawa · Masaki Murata · Masanori Nojima · Kumi Takasawa · Jiro Ogino · Yukimura Higashiura · Ayaka Sasaki · Yasutoshi Kimura · Toru Mizuguchi · Satoshi Tanaka · Koichi Hirata · Norimasa Sawada · Tadashi Hasegawa

Received: 1 July 2014 / Revised: 6 October 2014 / Accepted: 2 December 2014 / Published online: 14 December 2014

Abstract Biliary tract cancers have an extremely poor outcome, and specific diagnostic markers and effective treatments are needed urgently. In this study, we assessed the capacity of panel of immunohistochemical markers including claudin-18, maspin, and p53 to distinguish biliary tract carcinoma and biliary intraepithelial neoplasia (BilIN) from non-neoplastic epithelium. We performed a retrospective study of 66 biliary tract cancer specimens and 63 specimens with non-neoplastic lesions. Of the surgical specimens, 96.7 % with adenocarcinoma/BilIN were detected as neoplastic, and all 63 specimens histologically diagnosed as non-neoplastic lesion were detected as non-neoplastic with high sensitivity (91.1 %) and specificity (100 %). Of presurgical endobiliary forceps biopsy specimens, all with adenocarcinoma/BilIN and only 1 of the 19 with a non-neoplastic lesion were distinguished as neoplastic with high sensitivity (100 %) and specificity (94.7 %). Moreover, this panel provided good separation of neoplasm from malignancy-undetermined atypical epithelium (18/21, 85.7 %). This panel achieves a more reliable distinction of biliary tract cancers and BilINs from non-neoplastic epithelia in both surgical and biopsy specimens than immunohistochemical analysis with single antibodies and is useful in supporting a diagnosis of adenocarcinoma and BilIN.

Keywords Claudin-18 · Maspin · p53 · Human bile duct cancer · Early diagnosis

Electronic supplementary material The online version of this article (doi:10.1007/s00428-014-1705-4) contains supplementary material, which is available to authorized users.

Y. Keira · J. Ogino · T. Hasegawa
Departments of Surgical Pathology, Sapporo Medical University School of Medicine, Sapporo, Japan

A. Takasawa (✉) · M. Murata · K. Takasawa · Y. Higashiura · A. Sasaki · S. Tanaka · N. Sawada
Departments of Pathology, Sapporo Medical University School of Medicine, Sapporo, Japan
e-mail: atakasawa@sapmed.ac.jp

M. Nojima
Division of Advanced Medicine Promotion, The Advanced Clinical Research Center, The Institute of Medical Science, The University of Tokyo, Tokyo, Japan

Y. Kimura · T. Mizuguchi · K. Hirata
Departments of Surgery, Surgical Oncology, and Science, Sapporo Medical University School of Medicine, Sapporo, Japan

Introduction

The incidence of biliary tract cancers, comprising gallbladder, bile duct, and ampullary cancer, has been increasing worldwide over the past several decades and in the USA over the last decade [1, 2]. In Japan, the morbidity associated with these cancers has also increased, and more than 18,000 people died of this cancer in 2012 [3].

Generally, the overall prognosis for biliary tract cancer is poor. Although currently only surgical resection may be curative, the curative resection rate has remained low at approximately 40 % [4]. Therefore, early detection and preoperative confirmation of the malignant diagnosis is vitally important in improving prognosis [5]. The gold standard method of diagnosis requires endobiliary forceps biopsy and percutaneous liver biopsy. However, histopathological examination of biopsy tissues in clinical practice can be challenging because of a limited amount of material, crush artifacts, and the presence of confounding acute and chronic inflammatory epithelial changes [6, 7].

The need for accurate diagnostic methods has led to the exploration of immunohistochemical markers to distinguish

between benign atypia and malignancy [8–13]. In the present study, we examined the potential of three molecules, claudin-18 (cldn18), maspin, and p53, to serve as immunohistological diagnostic markers for bile duct cancers, biliary intraepithelial neoplasia (BilIN), and ampullary cancer, which can be difficult to diagnose by histology alone. BilIN is a flat-type premalignant or in situ neoplastic lesion of the biliary tract that was first documented in 2005 and has been recently included in the WHO classification of 2010 as intraductal papillary neoplasm of the bile duct (IPNB) [14–16]. BilIN occurs in intrahepatic and extrahepatic bile ducts and sometimes result from disorders of the biliary tract, such as hepatolithiasis, choledochal cysts, and primary sclerosing cholangitis. Biliary tract cancers progress through multistep carcinogenesis, with multiple molecular events such as KRAS and GNAS mutation and p53 overexpression, and BilIN and IPN are precursor lesions [15, 17]. BilIN is subdivided into BilIN-1, BilIN-2, and BilIN-3 according to the degree of cellular atypia and architectural disturbance. BilIN-1 and BilIN-2 correspond to low and intermediate grades, respectively. BilIN-3 is high grade and equivalent to carcinoma in situ.

Claudins are tight junction resident transmembrane proteins that are present in epithelial and endothelial cells and in derived neoplastic cells [18]. Aberrant expression of a number of claudins has been reported in various carcinomas [19, 20]. Cldn18 is detected in gastrointestinal and lung tissues [21–23]. In pancreatic ductal adenocarcinoma, cldn18 is overexpressed and has been identified as a potential diagnostic marker [24]. In the biliary tract, multivariable analysis demonstrated that positive cldn18 expression is an independent risk factor for lymph node metastasis [25]. Recently, we reported that cldn18 is primarily regulated at the transcriptional level via specific protein kinase C signaling pathways and that its expression is modified by DNA methylation [26].

Mammary serine protease inhibitor, otherwise known as maspin, is a member of the serine protease inhibitor superfamily and was identified as a tumor suppressor in mammary tissue in 1994 [27]. However, subsequent studies have revealed its tumor-suppressive properties to be complex and dependent on factors such as genetic background, type of cancer, and the expression of maspin (or lack thereof) in the corresponding normal tissue. Interestingly, both methylation and demethylation of the *maspin* promoter have been reported to influence its expression [28]. Some studies demonstrated an association between hypermethylation of the *maspin* promoter and loss of maspin expression in colonic and ovarian cancers [29, 30]. Others reported that demethylation was associated with maspin overexpression in gastric cancer [31]. In biliary tract cancer, demethylation of the *maspin* promoter and aberrant maspin expression has been reported [32]. In pancreatic ductal adenocarcinoma, overexpression of maspin is associated with lower postoperative survival [33]. In the gallbladder, use of an immunohistochemical panel including maspin has been reported to distinguish adenocarcinoma from benign/reactive epithelium [34].

Mutation of the *p53* gene is a key event in the carcinogenesis of many different types of tumors. The presence of this genetic abnormality in biliary tract cancer has been suggested in various investigations that used immunohistochemical and molecular epidemiological methods [35, 36].

Currently, accurate cancer detection including localization is needed to improve the prognosis of patients with bile duct cancers. In this study, we used immunohistochemical methods to document the expression of cldn18, maspin, and p53 in bile duct carcinomas, BilINs, and ampullary carcinoma in surgical specimens and analyzed the diagnostic utility of this immunohistochemical panel in presurgical bile duct biopsy specimens.

Materials and methods

Surgical specimens

A total of 66 biliary tract cancer specimens obtained by surgical excision from 1999 to 2011 were retrieved from the pathology file of Sapporo Medical University Hospital, Sapporo, Japan. Their clinicopathological characteristics are summarized in Table 1. Gallbladder cancer was excluded from the present study because presurgical biopsies had not been performed. The histological type of all cancers was adenocarcinoma. The cancer staging system was based on both the UICC classification (7th edition) and the Japanese Society of Biliary Surgery classification (fifth edition). Among the 66 adenocarcinomas, 25 (9 intrahepatic, 5 hilar extrahepatic bile duct, 7 distal extrahepatic bile duct, and 4 ampulla of Vater) had flat intraepithelial neoplastic lesions around invasive carcinomas. These intraepithelial lesions consisted of precursor lesions, that is, true BilIN, and superficial spreading lesions that were difficult to differentiate. Thus, in the present study, all intraepithelial components were classified as BilIN-1, BilIN-2, and BilIN-3 according to the degree of cell atypia. In addition, 63 specimens with non-neoplastic epithelia from cases of adenocarcinoma (25 intrahepatic, 10 hilar extrahepatic bile duct, 21 distal extrahepatic bile duct, and 7 ampulla of Vater) were selected as a control group. All slides were independently evaluated by three pathologists (KY, TA, and MM). Discordant cases were discussed, and a consensus was reached.

Immunohistochemical staining of surgical specimens

The hematoxylin and eosin (H&E)-stained slides from all cases were reviewed to select representative sections. New sections from paraffin blocks were examined by the labeled polymer method. Sections were deparaffinized, rehydrated, moistened with phosphate-buffered saline (PBS; pH 7.4),

Table 1 Clinicopathological features of biliary tract cancers

Total (N=66)		Intrahepatic bile duct carcinoma (N=27)		Extrahepatic bile duct carcinoma (N=32)		Ampullary carcinoma (N=7)	
Age (range, median)	39–84, 68.5	T grade (UICC)		T grade (UICC)		T grade (UICC)	
Sex		T1/T2	22	Tis/T1/T2	18	Tis/T1/T2	4
Male	47	T3/T4	5	T3/T4	14	T3/T4	3
Female	19	T grade[b]		T grade[b]		T grade[b]	
Location		T1/T2	14	T1/T2	11	T1/T2	2
Intrahepatic	27	T3/T4	13	T3/T4	21	T3/T4	5
Extrahepatic	32	Lymph node metastasis		Lymph node metastasis		Lymph node metastasis	
Hilar	11	Negative	24	Negative	20	Negative	4
Distal	21	Positive	3	Positive	12	Positive	3
Ampulla of Vater	7	Stage group (UICC)		Stage group (UICC)		Stage group (UICC)	
Tumor size		I/II	20	0/IA/IB/II	15	0/IA/IB/II	2
≦3 cm	29	III/IV	7	IIA/IIB/IIIA/IIIB	17	IIA/IIB/IIIA/IIIB	5
>3 cm	25	Stage group[b]		Stage group[b]		Stage group[b]	
Unknown	12	I/II	13	I/II/III	17	I/II/III	3
Histological type		III/IVA/IVB	14	IVA/IVB	15	IVA/IVB	4
Well	33	Lymphatic invasion		Lymphatic invasion		Lymphatic invasion	
Moderately	16	Negative	–	Negative	13	Negative	2
Poorly	17	Positive	–	Positive	19	Positive	5
BilIN[a]		Venous invasion		Venous invasion		Venous invasion	
BilIN-1	8	Negative	18	Negative	16	Negative	3
BilIN-2	11	Positive	9	Positive	23	Positive	4
BilIN-3	6			Interstitial connective tissue		Interstitial connective tissue	
				Medullary	4	Medullary	1
				Intermediate	20	Intermediate	6
				Scirrhous	8	Scirrhous	0

[a] Flat intraepithelial neoplastic lesion around invasive carcinoma classified as BilIN-1, BilIN-2, and BilIN-3 according to the degree of cell atypia

[b] General rules for surgical and pathological studies on cancer of the biliary tract (fifth edition) by the Japanese Society of Biliary Surgery

and then pretreated in an autoclave at 121 °C for 5 min in 10 mM citrate buffer (pH 6.0), followed by 30 min incubation with antibodies to the following antigens in an automated immunostaining system (Dako Autostainer; Dako, Carpinteria, CA, USA): cldn18 (Invitrogen, Carlsbad, CA; polyclonal, ×100), maspin (BD, Franklin Lakes, NJ; G167-70, ×50), and p53 (Dako, DO-7, ×50). Maspin immunoreactivity was independently evaluated in the cytoplasm (C) or nucleus (N). The intensity of staining was assessed as strong (3), moderate (2), weak (1), or negative (0). The proportion of neoplastic cells stained was recorded as 0 (no staining), 1 (1–10 %), 2 (11–20 %), 3 (21–30 %), 4 (31–40 %), 5 (41–50 %), 6 (51–60 %), 7 (61–70 %), 8 (71–80 %), 9 (81–90 %), or 10 (91–100 %). Because neoplasm heterogeneity caused variable immunoreactivity in each case, we established a multiplication score for improvement of accuracy: The minimum score was intensity 0×proportion 0 (multiplication score 0), and the maximum was intensity 3×proportion 10 (multiplication score 30). Several representative fields were examined.

Double-staining immunohistochemistry

For double immunostaining, paraffin-embedded tissue sections were deparaffinized in xylene (10 min, two times) and rehydrated through a graded ethanol series. Antigen retrieval was performed by immersing sections in 10 mM Tris-1 mM EDTA buffer (pH 9.0) and boiling in a microwave oven (95 °C, 30 min). After washing of the sections with PBS (5 min, three times), they were allowed to cool at room temperature. They were then incubated in 3 % hydrogen peroxide for 10 min to inactivate endogenous peroxidase. After washing in PBS (5 min, three times), they were incubated with anti-maspin antibody (BD, G167-70, ×50) overnight at 4 °C. The following day, the sections were washed in PBS (5 min, three times), and immunostaining was performed by a standard immunoperoxidase technique (Histofine SAB-PO Kit, Nichirei Co., Tokyo, Japan) with a BCIP/NBT substrate system (Dako Laboratories) as chromogen, according to the manufacturer's instructions. After the sections were washed in distilled water (5 min, three times), antigen retrieval

was performed by immersing the sections in 10 mM Tris-1 mM EDTA buffer (pH 9.0) and boiling in a microwave (95 °C, 10 min). The sections were washed with PBS (5 min, three times) and allowed to cool to room temperature. Subsequently, the sections were incubated with anti-cldn18 antibody (Invitrogen, polyclonal, ×100) overnight at 4 °C. The following day, after the sections were washed in PBS (5 min, three times), immunostaining was performed with the Dako REAL™ EnVision™ Detection System (Dako ChemMate, Glostrup, Denmark) with diaminobenzidine (Dako Laboratories) as the chromogen, according to the manufacturer's instructions. Sections were then counterstained with hematoxylin, dehydrated, and mounted.

Immunohistochemical analysis of presurgical biopsy specimens

As an additional study, immunohistochemical analysis was performed on 58 samples (18 adenocarcinomas, 21 malignancy-undetermined atypical epithelia, and 19 non-neoplastic lesions) taken from presurgical extrahepatic bile duct forceps biopsies and 7 samples (4 adenocarcinomas and 3 non-neoplastic lesions) taken from presurgical percutaneous biopsies. All specimens of malignancy-undetermined atypical epithelium showed nuclear atypia and turned out to be adenocarcinoma by histological examination of the subsequent surgical specimens. The 19 specimens with non-neoplastic lesions from endobiliary forceps biopsies comprised 5 specimens of IgG4-related sclerosing cholangitis, 5 of primary sclerosing cholangitis, and 9 of nonspecific fibrosis/inflammation. All three specimens of non-neoplastic lesions from percutaneous liver biopsies concerned nonspecific fibrosis/inflammation. None of the patients had a stent when the biopsy was performed. The immunohistochemical protocol was the same as that described above. Because of the small amount of epithelium in biopsy specimens, any immunoreactivity in epithelial cells was regarded as positive regardless of the multiplication score. A case with one or more positive atypical epithelia was given a binary value of 1, while absence of positive atypical epithelia was given a binary value of 0.

Statistics

A three-step analysis was used for the surgical specimens. In the first step, cutoff values were calculated for the multiplication scores of cldn18, maspin (N), and p53 that would distinguish the following: (i) adenocarcinoma from non-neoplastic epithelium, (ii) BilIN from non-neoplastic epithelium, and (iii) neoplasm (adenocarcinoma/BilIN) from non-neoplastic epithelium. In the second step, other cutoff values were calculated for the combined multiplication scores from cldn18, maspin (N), and p53 that would distinguish neoplastic (adenocarcinoma/BilIN) from non-neoplastic epithelium. Third, for every antibody, the multiplication score was converted to its respective binary value using cutoff values obtained in the first step as the threshold. The score with the highest sensitivity and specificity was used to define the receiver operator characteristic (ROC) curve, and the area under the receiver operator characteristic curve (AUC) was calculated. We used 95 % confidence intervals (CIs) to test the hypothesis that AUC is 0.5. For presurgical biopsy specimens, ROC curve analysis was performed to calculate the best binary value in the combination of cldn18, maspin (N), and p53. All statistical analyses were performed with SPSS statistics ver. 20.

Results

Patient characteristics

The study population of 66 patients with biliary tract cancers consisted of 47 men and 19 women, ranging at the time of diagnosis between 39 and 84 years of age (Table 1). The median age of the patients was 68.5 years. The number of patients according to UICC stage was as follows: intrahepatic bile duct cancer I/II $n=20$ and III/IV $n=7$, and extrahepatic bile duct and ampullary carcinoma 0/IA/IB/II $n=17$ and IIA/IIB/III/IV $n=22$. Cases of BilIN were classified as 8 of BilIN-1, 11 of BilIN-2, and 6 of BilIN-3 as described in the "Materials and methods." None of the patients had papillary lesions identified as IPNB.

Cldn18 expression in surgical specimens

First, we examined the immunochemistry of the surgical specimens for cldn18, maspin, and p53 independently. In the biliary tract tissues, immunostaining of cldn18 was observed in the basolateral membrane of the neoplastic cells (Fig. 1). In contrast, staining for cldn18 was almost absent in non-neoplastic epithelial cells. To maximize reproducibility and accuracy of the immunohistochemical evaluation, we defined a parameter, designated as the multiplication score, which was calculated by multiplying intensity (4 grades) and proportion (11 grades) of immunoreactivity. The multiplication scores for cldn18 in adenocarcinoma, BilIN-3, BilIN-2, BilIN-1, and non-neoplastic epithelium were (mean±SD/median) 22±6.8/24, 26±2.8/27, 25±6.1/27, 23±9.1/27, and 0.97±2.3/0, respectively (Table 2).

In adenocarcinomas, the multiplication score was lower because differentiation of the neoplasm was poor. Multiplication scores in well, moderately, and poorly differentiated adenocarcinoma were (mean±SD/median) 23±5.8/24, 21±8.2/24, and 17±7.5/18, respectively (Table 3

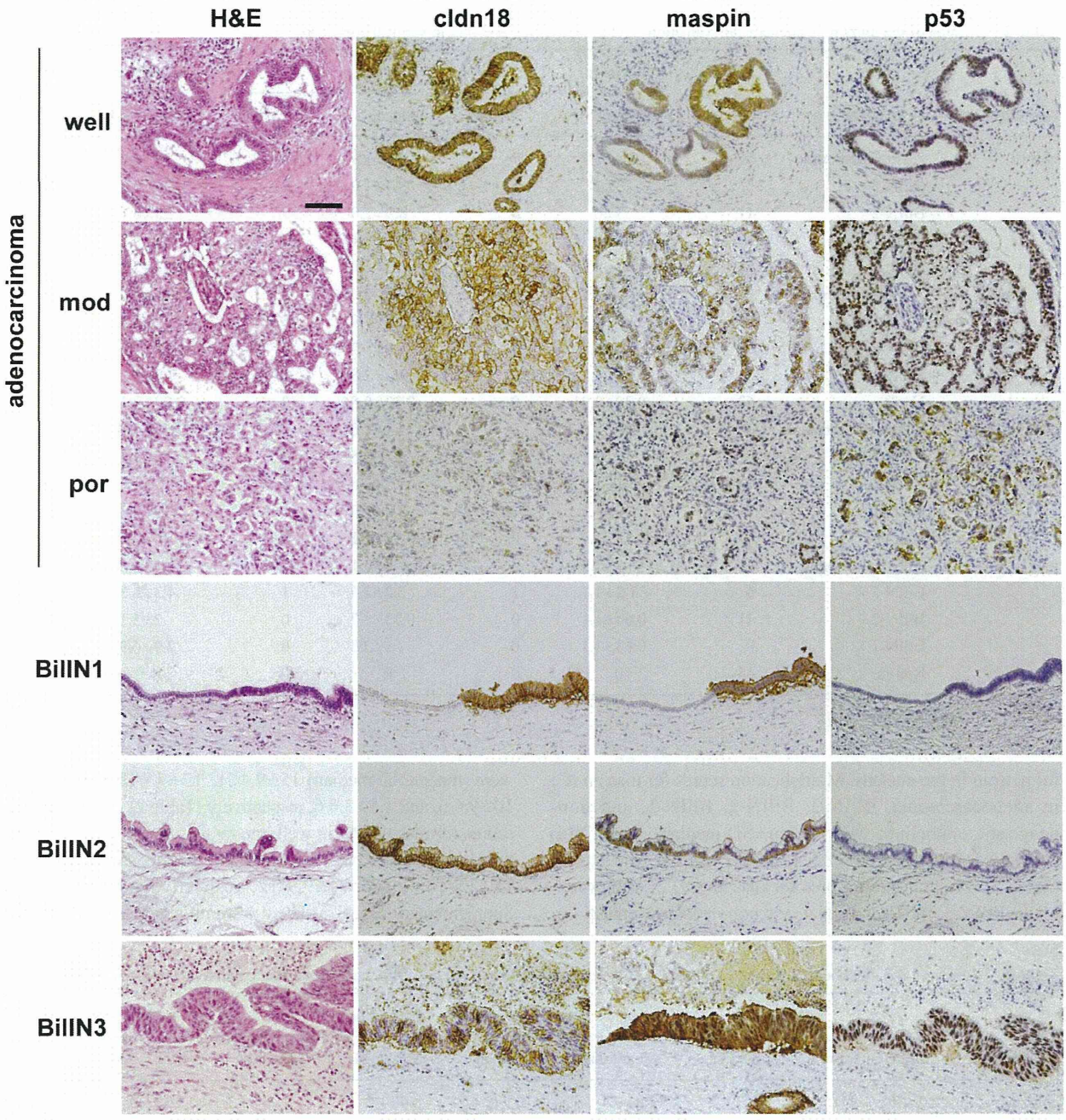

Fig. 1 H&E staining and immunohistochemical staining in surgical specimens of well, moderately (mod), and poorly (por) differentiated bile duct adenocarcinoma and BilIN-1, BilIN-2, and BilIN-3. Cldn18 was expressed on basolateral membranes of the epithelial cells in adenocarcinoma and BilIN-1, BilIN-2, and BilIN-3. Maspin was also expressed in both the cytoplasm and nucleus of the epithelial cells in adenocarcinoma and BilIN-1, BilIN-2, and BilIN-3. p53 was expressed in the nucleus of the epithelial cells in some specimens of adenocarcinoma and BilIN-2 and BilIN-3. In the non-neoplastic epithelial cells adjacent to BilIN, none of the three antibodies caused staining

and Supplementary Fig. S1). Cldn18 was distributed along the entire cell membrane of most cells in well-differentiated adenocarcinomas and expressed at least in part on the cell surfaces of poorly differentiated adenocarcinoma cells (Fig. 1). There were no significant changes in the cldn18 expression patterns in BilIN-1, BilIN-2, and BilIN-3.

Maspin expression in surgical specimens

Immunostaining of maspin was observed in both the cytoplasm and nucleus of the neoplastic cells (Fig. 1). Apart from bile duct epithelium, some non-neoplastic hepatic cells and duodenal epithelial cells were positive

Table 2 Results of the immunohistochemical evaluation of cldn18, maspin, and p53 in surgical specimens

			Intensity		Proportion		Multiplication score	
Antibody	Histological type	Number	Mean±SD	Median	Mean±SD	Median	Mean±SD	Median
cldn18	Adenocarcinoma	66	2.8±0.5	3	7.7±1.9	8	22±6.8	24
	BilIN-3	6	3±0	3	8.7±1.0	9	26±2.8	27
	BilIN-2	11	3±0	3	8.3±2.0	9	25±6.1	27
	BilIN-1	8	2.6±0.70	3	8.1±2.1	9	23±9.1	27
	Non-ne	63	0.48±0.73	0	0.73±1.6	0	0.97±2.3	0
Maspin (C)	Adenocarcinoma	66	2.3±1.2	3	5.0±3.2	5.5	14±9.7	15
	BilIN-3	6	2.7±0.5	3	6.2±2.9	6	17±9.5	15
	BilIN-2	11	2.3±1.1	3	5.0±3.7	5	15±11	15
	BilIN-1	8	1.6±1.3	2	2.6±2.8	2	7.3±8.6	4
	Non-ne	63	0.35±0.91	0	0.33±0.85	0	0.79±2.1	0
Maspin (N)	Adenocarcinoma	66	2.5±1.0	3	5.1±3.0	6	15. ± 9.4	18
	BilIN-3	6	3.0±0	3	5.7±1.6	6.5	17±4.8	19.5
	BilIN-2	11	2.0±1.3	3	4.5±3.6	5	13±11	15
	BilIN-1	8	1.9±1.3	2.5	3.8±3.0	3	10±9.6	6
	Non-ne	63	0.57±1.1	0	0.57±1.1	0	1.5±3.0	0
p53	Adenocarcinoma	66	1.7±1.3	2	2.7±3.1	1	7.4±9.5	3
	BilIN-3	6	1.2±1.1	1	2.2±2.4	1	4.3±6.3	1.5
	BilIN-2	11	0.64±1.1	0	0.73±1.7	0	2±5.1	0
	BilIN-1	8	0.63±1.1	0	1±2.3	0	2.9±6.9	0
	Non-ne	63	0	0	0	0	0	0

Non-ne non-neoplastic epithelium

for maspin in the nucleus. Multiplication scores for maspin (C) in adenocarcinoma, BilIN-3, BilIN-2, BilIN-1, and non-neoplastic epithelium were (mean±SD/median) 14±9.7/15, 17±9.5/15, 15±11/15, 7.3±8.6/4, and 0.79±2.1/0, respectively (Table 2). Multiplication scores for maspin (N) in adenocarcinoma, BilIN-3, BilIN-2, BilIN-1, and non-neoplastic epithelium were (mean±SD/median) 15±9.4/18, 17±4.8/19.5, 13±11/15, 10±9.6/6, and 1.5±3.0/6, respectively (Table 2). Multiplication scores for maspin (N) in well, moderately, and poorly differentiated adenocarcinoma were (mean±SD/median) 17±8.2/21, 12±10/10.5, and 14±9.9/12, respectively (Table 3 and Supplementary Fig. S1). There were no significant differences

Table 3 Results of the immunohistochemical evaluation of well, moderately, and poorly differentiated adenocarcinoma in surgical specimens

			Intensity		Proportion		Multiplication score	
Antibody	Differentiation	Number	Mean±SD	Median	Mean±SD	Median	Mean±SD	Median
cldn18	Well	33	2.9±0.4	3	8.0±1.5	8	23±5.8	24
	Moderately	16	2.7±0.7	3	7.8±2.2	8	21±8.2	24
	Poorly	17	2.2±0.7	2	7.2±2.1	8	17±7.5	18
Maspin (C)	Well	33	2.5±1.0	3	5.9±3.0	7	17±9.5	21
	Moderately	16	1.9±1.2	2.5	4.1±3.1	4	10±9.2	8.5
	Poorly	17	2±1.3	3	4±3.1	4	11±9.2	12
Maspin (N)	Well	33	2.6±0.8	3	5.8±2.6	7	17±8.2	21
	Moderately	16	2.1±1.3	3	4.1±3.4	3.5	12±10	10.5
	Poorly	17	2.4±1.0	3	4.8±3.2	5	14±9.9	12
p53	Well	33	1.8±1.3	2	2.9±3.2	1	7.8±9.6	3
	Moderately	16	1.6±1.2	2	2.9±3.2	1	7.5±9.3	2.5
	Poorly	17	1.6±1.3	2	2.1±2.8	1	5.8±8.7	2

in the scores among adenocarcinomas (all histological types; data not shown).

p53 expression in surgical specimens

p53 was expressed in the nucleus in some adenocarcinomas and a few specimens with BilIN-2 and BilIN-3 (Fig. 1). Multiplication scores in specimens with adenocarcinoma, BilIN-3, BilIN-2, BilIN-1, and non-neoplastic epithelium were (mean±SD/median) 7.4±9.5/3, 4.3±6.3/1.5, 2.0±5.1/0, 2.9±6.9/0, and 0/0, respectively (Table 2). For each neoplasm, the multiplication scores for p53 were lower than those for cldn18 and maspin, but p53 was the most specific of the three markers (Table 2). Multiplication scores in well, moderately, and poorly differentiated adenocarcinoma were (mean±SD/median) 7.8±9.6/3, 7.5±9.3/2.5, and 5.8±8.7/2, respectively (Table 3 and Supplementary Fig. S1).

Diagnostic value of cldn18, maspin, and p53 in surgical specimens

To distinguish neoplasms from non-neoplastic epithelium in the surgical specimens from patients with biliary tract cancers, we calculated the AUC for cldn18, maspin, and p53, as described in the "Materials and methods" (Fig. 2a). The AUC for cldn18 was 0.992 [95 % CI, 98.3 to 100] (Fig. 2b). A cutoff value of 6 produced the highest accuracy (minimal number of false-negative and false-positive results); sensitivity and specificity were 95.6 and 96.8 %, respectively. There was no significant difference in the scores between BilIN-1–3, so BilIN-1–3 were referred to collectively as "BilIN" (Fig. 2c). As shown in the upper panel of Fig. 2c, 87 of 91 (95.1 %) specimens with adenocarcinoma/BilIN (63 of 66 with adenocarcinoma and 24 of 25 with BilIN) were detected as neoplastic. Among specimens with non-neoplastic epithelium, 61 of 63 (96.8 %) were detected as non-neoplastic. The AUC for maspin (N) was 0.879 [95 % CI, 82.5 to 93.3] (Fig. 2b). A cutoff value of 1 gave the highest accuracy; sensitivity and specificity were 85.6 and 77.8 %, respectively. As shown in the third panel of Fig. 2c, 78 of 91 (85.7 %) specimens with adenocarcinoma/BilIN (58 of 66 with adenocarcinoma and 20 of 25 with BilIN) were detected as neoplastic. Among the specimens with non-neoplastic epithelium, 49 of 63 (77.8 %) were detected as non-neoplastic. The AUC for p53 was 0.806 [95 % CI, 73.7 to 87.4] (Fig. 2b). A cutoff value of 1 produced the highest accuracy; sensitivity and specificity were 61.1 and 100 %, respectively. As shown in the bottom panel of Fig. 2c, 56 of 91 (61.5 %) specimens with adenocarcinoma/BilIN (47 of 66 with adenocarcinoma and 9 of 25 with BilIN) were detected as neoplastic. Among specimens with non-neoplastic epithelium, all 63 were detected as non-neoplastic. For distinguishing adenocarcinoma from non-neoplastic epithelium or BilIN from non-neoplastic epithelium, ROC curves showed that all the three markers were highly accurate (Supplementary Figs. S2A and S2B).

Next, we obtained additional scores by combining the multiplication scores for cldn18, maspin (N), and p53 and analyzed the new scores to distinguish neoplastic from non-neoplastic tissues. The AUC for the combined multiplication score was 0.996 [95 % CI, 98.8 to 100] (Supplementary Fig. S3A). A cutoff value of 15 had the highest specificity; sensitivity and specificity were 96.6 and 100 %, respectively. A cutoff value of 12 had the highest sensitivity; sensitivity and specificity were 100 and 96.8 %, respectively (Supplementary Fig. S3A). When all specimens were differentiated by a cutoff value of 15, 88 of 91 (96.7 %) specimens with adenocarcinoma/BilIN were detected as neoplastic, and all 63 specimens with histologically diagnosed non-neoplastic epithelium were detected as non-neoplastic (Supplementary Fig. S3B). These results indicate that the strategy of combining the three multiplication scores successfully distinguished neoplasms from non-neoplastic epithelia in the surgical specimens of biliary tract carcinoma.

For convenience, we employed an additional step. Before combining the three parameters for cldn18, maspin (N), and p53, we converted each of the multiplication scores to binary values (0 for immuno-negative and 1 for immuno-positive) on the basis of the best cutoff values calculated above. With the binary values for cldn18, maspin (N), and p53, we calculated the AUC and analyzed the new scores to distinguish neoplasms from non-neoplastic tissues (Fig. 3). After these processes, the AUC was 0.989 [95 % CI, 97.8 to 99.9] (Fig. 3a). As shown in Fig. 3b, the best cutoff score was 2, 81 of 91 (89.0 %) specimens with adenocarcinoma/BilIN and none with non-neoplastic epithelium were distinguished as neoplastic, and sensitivity and specificity were 91.1 and 100 %, respectively. At a cutoff value of 1, all 91 specimens with adenocarcinoma/BilIN and 15 of 63 (23.8 %) with non-neoplastic epithelium were distinguished as neoplastic; sensitivity and specificity were 100 and 74.6 %, respectively. At a cutoff value of 3, 41 of 91 (45.1 %) specimens with adenocarcinoma/BilIN and none with non-neoplastic epithelium were distinguished as neoplastic; sensitivity and specificity were 51.1 and 100 %, respectively.

Diagnostic value of cldn18, maspin, and p53 in presurgical endobiliary forceps biopsy specimens

Next, we examined whether this analysis is applicable to presurgical endobiliary forceps biopsy specimens because they are the most important source for both clinical diagnosis and rapid intraoperative diagnosis. The immunostaining patterns of the presurgical endobiliary forceps biopsy specimens were similar to those of the surgical specimens (Fig. 4a). In biopsy specimens, we observed that some epithelia without apparent dysplasia, including intestinal epithelium, were

a

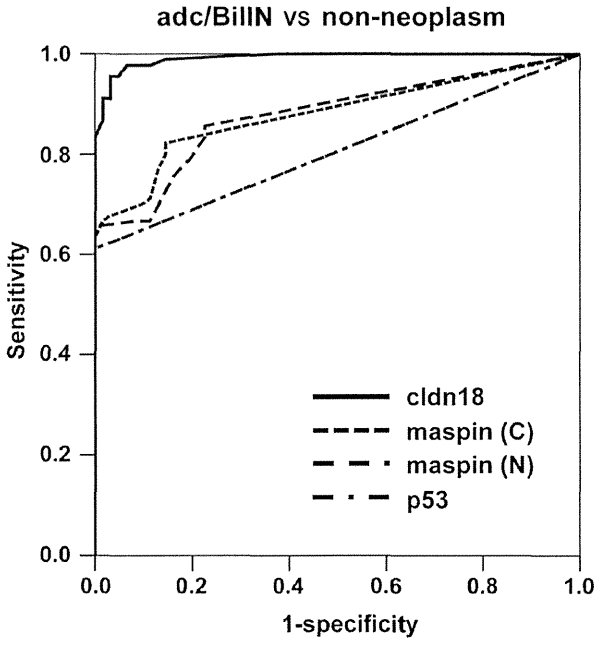

b

		95%CI	
	AUC	Lower	Upper
cldn18	0.992	0.983	1.000
maspin (C)	0.881	0.826	0.935
maspin (N)	0.879	0.825	0.933
p53	0.806	0.737	0.874

score	Best cutoff	Sensitivity	Specificity
cldn18	≥6	0.956	0.968
maspin (C)	≥1	0.822	0.857
maspin (N)	≥1	0.856	0.778
p53	≥1	0.611	1.000

c

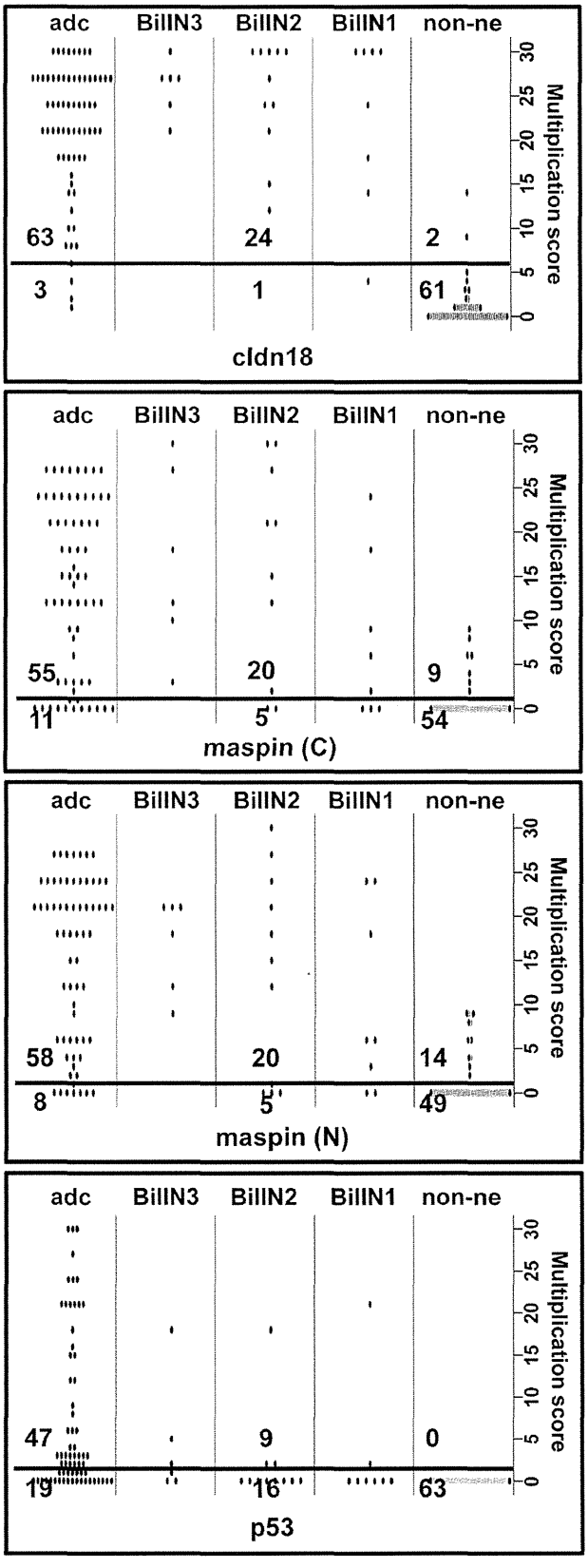

◀ **Fig. 2** ROC curve analysis of cldn18, maspin, and p53 in surgical specimens. **a** ROC curves were calculated according to multiplication scores that represented the degrees of immunoreactivity with a scale of 0 to 30 for each antibody as described in "Materials and methods." Immunoreactivity against maspin was separately evaluated in the cytoplasm (C) and nucleus (N). Cutoff values were calculated from the ROC curves to distinguish adc/BilIN from non-neoplastic epithelium (*non-ne*). **b** Accuracy was measured by the AUC. The 95 % CIs for AUC and best cutoff values with the highest accuracy are summarized in the tables. **c** *Dot plots* show the distribution of multiplication scores for each antibody. In each panel, the *bold horizontal line* represents the best cutoff value to divide the cases into two groups, adc/BilIN (*above the line*) and non-ne (*below the line*). *CI* confidence interval

positive for maspin (5 of 22 non-neoplastic cases). However, we classified these as negative for maspin because H&E staining clearly demonstrated them as non-neoplastic (data not shown). To distinguish neoplasms from non-neoplastic epithelia, we analyzed the combined scores from the binary values for cldn18, maspin (N), and p53, as described for the surgical specimens. The AUC was 0.990 [95 % CI, 0.964–100] (data not shown). As shown in Figs. 4b, c, and d, at a cutoff value of 1, all 18 specimens with adenocarcinoma/BilIN and 4 of 19 with non-neoplastic epithelium were distinguished as neoplastic. The sensitivity and specificity were 100 and 78.9 %, respectively. At a cutoff value of 2, all 18 specimens with adenocarcinoma/BilIN and 1 of 19 with non-neoplastic epithelium were distinguished as neoplastic. The sensitivity and specificity were 100 and 94.7 %. When the cutoff value was set at 3, 11 of 18 specimens with adenocarcinoma/BilIN and none of those with non-neoplastic epithelium were distinguished as neoplastic. The sensitivity and specificity were 61.1 and 100 %, respectively. A cutoff value of 2 had the highest sensitivity and specificity, and the score provided good separation of neoplasm from malignancy-undetermined atypical epithelium (18/21, 85.7 %) in cases that showed nuclear atypia but could not be proven as adenocarcinoma with a biopsy. We examined seven percutaneous liver biopsy specimens and found that a cutoff value of 2 had the highest sensitivity and specificity (Supplementary Fig. S4).

Double staining of cldn18 and maspin

We examined 14 surgical specimens of biliary tract cancer by double staining for cldn18 and maspin. The staining pattern was coincident with those expected from the single staining patterns of cldn18 and maspin (Fig. 4e). Some specimens of neoplastic epithelium were immunoreactive for both cldn18 and maspin (12/14, 86 %); others were reactive only for cldn18 (2/14, 14 %), indicating that all examined biliary tract adenocarcinomas were positive for at least cldn18 or maspin. Among the 14 specimens, 9 had BilINs and all were positive for at least one marker. All of the specimens with BilIN-1 (3/3) and BilIN-3 (3/3) and 1/3 of those with BilIN-2 were double-

a

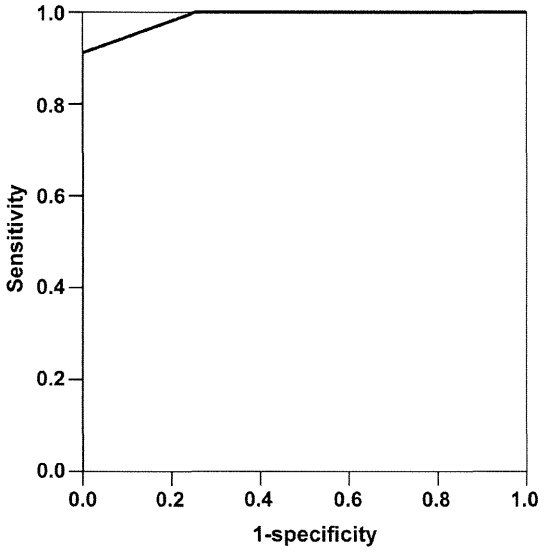

AUC	95%CI Lower	Upper
0.989	0.978	0.999

b

		Sensitivity	Specificity
Score (binary value)	≥1	1.000	0.746
	≥2	0.911	1.000
	≥3	0.511	1.000

		adc/BilIN	non-neoplasm
Score (binary value)	0	0	48
	1	10	15
	2	40	0
	3	41	0
Total		91	63

Fig. 3 ROC curve analysis in surgical specimens performed by using combined parameters of cldn18, maspin, and p53. **a** The ROC curve was calculated according to the combined binary values of the multiplication scores for each antibody. Briefly, each of the multiplication scores was converted to a binary value (0 for immuno-negative and 1 for immuno-positive) on the basis of the best cutoff values for each antibody (refer to Fig. 2b). Then, the binary values were combined, to give scores of 0: all immuno-negative to 3: all immuno-positive. Cutoff values were calculated from the ROC curve to distinguish adc/BilIN from non-neoplasm. Accuracy was measured by AUC. **b** Sensitivity and specificity for each cutoff value are summarized. With a cutoff value of 2, where any two antibodies produced immuno-positive staining, 81/91 adc/BilIN and none of non-neoplasm were evaluated as neoplastic with the highest sensitivity and specificity

positive, and 2/3 of those with BiliN-2 were positive only for cldn18. In contrast, most non-neoplastic specimens were negative for both cldn18 and maspin, except for one that was positive for maspin (1/14, 7 %).

Discussion

The aim of this study is to provide a new approach to distinguish biliary tract carcinoma and BilIN from non-neoplastic epithelia with high sensitivity and specificity. We achieved this by a combination of immunohistochemical staining for cldn18, maspin, and p53. Expression of these three antigens has been reported in association with biliary tract carcinomas [20, 25, 32, 34–36], but immunostaining of each individual marker seems to be insufficient to distinguish biliary tract carcinoma/BilIN from non-neoplastic epithelia with certainty. For example, some diagnoses remained controversial if staining for cldn18 or maspin was weakly positive or if cldn18 was detected only in the cytoplasm, even though biliary tract carcinoma/BilIN is usually thought to overexpress cldn18 and maspin [20, 32, 34]. In addition, the prevalence of p53 expression in biliary tract carcinoma/BilIN is relatively low (approximately 30 % at most) with heterogeneous staining patterns even in a single specimen, although the p53 nuclear staining pattern is conspicuous and easy to evaluate in adenocarcinoma. Considering these advantages and disadvantages, we used a panel of all three immunohistochemical markers to reliably detect biliary tract carcinoma/BilIN.

First, we examined surgical specimens of biliary tract cancer by immunochemical staining for each marker, independently. Staining with each of the three antibodies seemed to demonstrate lack of homogeneity within an individual adenocarcinoma. In particular, almost every adenocarcinoma in the present study showed variable intensity and proportion of staining for cldn18 and maspin, not in association with histological differences. This may be attributed to genetic heterogeneity as neoplasms are genetically heterogeneous (interindividually and intraindividually), which is closely related to their progression and treatment response [34].

In the present study, we defined a parameter to maximize the reproducibility and accuracy of the immunohistochemical evaluation. This parameter, designated as the multiplication score, was calculated by multiplying the intensity (4 grades) and proportion (11 grades) of immunoreactivities for each antibody. All ROC curves revealed that sensitivity and specificity of the three markers are high enough to distinguish biliary tract adenocarcinomas/BilIN from non-neoplastic epithelia. Individually, maspin (N) immunostaining showed relatively high sensitivity (85.6 %) and specificity (77.8 %) in detecting adenocarcinoma and BilIN. p53 immunostaining showed the highest specificity (100 %), but the sensitivity was low (61 %). Cldn18 immunostaining also showed markedly high sensitivity (95.6 %) with a high specificity of 96.8 %, which would result from the high cutoff value of 6. Focal and weak cldn18-positive staining was detected in a small number of non-neoplastic epithelia, especially in the presence of reactive changes. Therefore, use of cldn18 or maspin alone may lead to an inadequate differentiation between non-neoplastic epithelia and neoplasms. Because both false-positive and false-negative results should be avoided as much as possible in medical practice, a panel of antibodies against all three markers, cldn18, maspin, and p53, should be used to increase diagnostic sensitivity and specificity. In fact, the combined multiplication score of the three markers improved the accuracy, as compared to the three individual scores (Fig. 2 and Supplementary Fig. S3B).

The combined multiplication score successfully distinguished neoplasms from non-neoplastic epithelia in the surgical specimens of the biliary tract; however, the scores were complicated to calculate and inconvenient for clinical application. Therefore, before combining the three parameters for cldn18, maspin (N), and p53, we converted each of the multiplication scores to binary values (0 for immuno-negative and 1 for immuno-positive) on the basis of the cutoff values that were calculated from the respective ROC curves. The binary values of staining for cldn18, maspin (N), and p53 were then combined to obtain an additional score. Binary processing of multiplication scores did not impair the high sensitivity and specificity of the original scores. For the combined binary values, cutoff values of 2 or 3, denoting immune-positivity for two or three antibodies, provided the highest sensitivity and specificity (91.1 and 100 %, respectively).

In the analysis of presurgical biopsy specimens, we divided the specimens into three groups on the basis of histology (adenocarcinoma/BilIN, malignancy-undetermined atypical epithelium, and non-neoplastic epithelium), because the condition of the biopsy specimens varied as described above which made it difficult to classify them precisely into multiple stages as we did with the surgical specimens. Among the groups, the patients with a final diagnosis of "malignancy-

Fig. 4 **a** H&E staining and immunohistochemical staining in three presurgical endobiliary forceps biopsy specimens with adenocarcinoma (adc)/BilIN and non-neoplasm. The immunostaining patterns were almost identical to those in the surgical specimens. **b** Immunohistochemical staining results based on the binary values to give scores of 0: all immuno-negative to 3: all immuno-positive. **c** The sensitivity and specificity for each cutoff value to distinguish adenocarcinoma (adc)/BilIN from non-neoplasm are summarized. **d** The sensitivity and specificity for each cutoff value to distinguish atypical epithelium from non-neoplasm are summarized. **e** Double immunohistochemical staining of cldn18 and maspin in the surgical specimens. The staining patterns of cldn18 (*brown*) and maspin (*blue*) were coincident with those expected from staining for each individually. A non-neoplastic gland was negative for both cldn18 and maspin (*asterisk*)

a

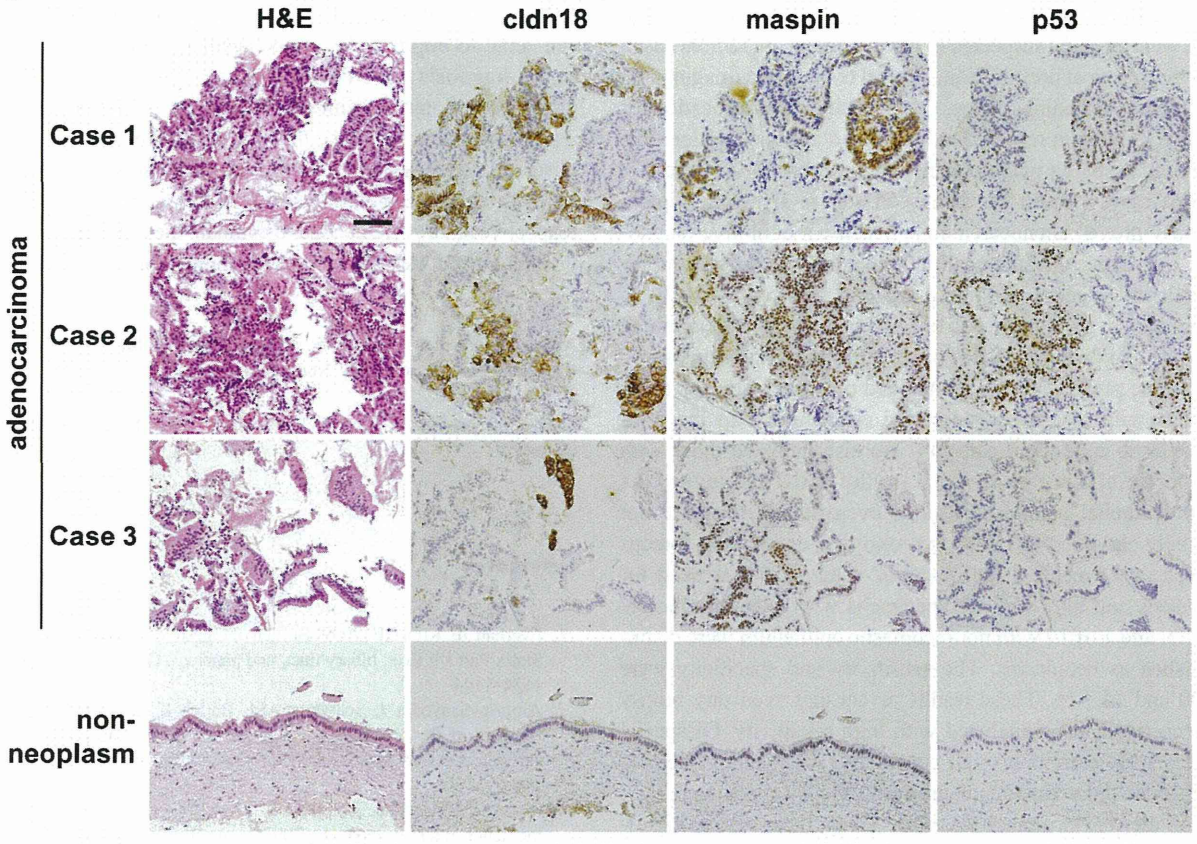

b

		adc/BilIN	atypical epithelium	non-neoplasm
Score (binary value)	0	0	1	15
	1	0	2	3
	2	7	6	1
	3	11	12	0
Total		18	21	19

c

adc vs non-neoplasm		Sensitivity	Specificity
Score (binary value)	≥1	1.000	0.789
	≥2	1.000	0.947
	≥3	0.611	1.000

d

atypical vs non-neoplasm		Sensitivity	Specificity
Score (binary value)	≥1	0.952	0.789
	≥2	0.857	0.947
	≥3	0.571	1.000

e

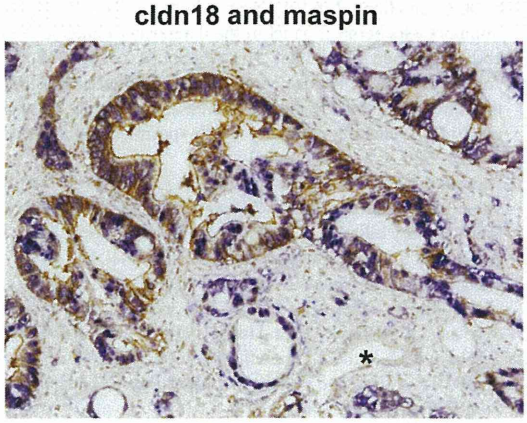

undetermined atypical epithelium" were not biopsy-proven but were strongly suspected of having malignant tumors based on their clinical presentation, clinical course, and imaging and examination findings. Those cases resulted in an indication for surgery and then received a definitive diagnosis of adenocarcinoma based on pathological examinations. We believe that these cases should be discussed separately from typical biopsy-proven adenocarcinoma, because a definitive diagnosis on suspected adenocarcinoma biopsy is important for treatment selection including surgical resection as early as possible. In this study, 85.7 % of malignancy-undetermined atypical epithelium (18/21) was differentiated as neoplastic.

In the present study, we included presurgical biopsy specimens with reactive/regenerative epithelium into the non-neoplastic epithelium category. We also included those with superficial spread lesions in the BilIN category as intraepithelial neoplastic lesions even though they are not usually classified this way. In presurgical endobiliary forceps biopsy specimens, a binary cutoff value of 2 was used for analysis and all 18 of the specimens with adenocarcinoma/BilIN and 1 of 19 with non-neoplastic epithelium were distinguished as neoplasms. The sensitivity and specificity were 100 and 94.7 %. These results reveal that even tiny biopsy specimens can be analyzed with high sensitivity. Of special note is the extremely high specificity, which could help to minimize indeterminate diagnoses in biopsy specimens.

In the statistical analysis of this study, there was no significant difference between BilIN-2 and BilIN-3 by using either each single marker or the panel of the three markers. To date, a number of candidate markers have been examined, some of which are expressed as early as BilIN-1, while others are only expressed from BilIN-2. For example, 25 % of BilIN-1 has been reported to carry a mutation in RAS genes [17]. BilIN-1/BilIN-2 is a neoplastic proliferation that should be followed as a precursor lesion that may progress to BilIN-3 and adenocarcinoma through multiple stages [15]. The detection of BilIN-1/BilIN-2 can be expected to identify high-risk cases, which might increase its clinical importance in the future even though further study is necessary.

We went on to perform the first reported evaluation of the efficiency of dual staining for cldn18/maspin in the diagnosis of bile duct adenocarcinoma in the surgical specimens. The difference in localization (membranous for cldn18; nuclear and cytoplasmic for maspin) and the two-colored chromogenic reaction (brown for cldn18 and blue for maspin) enables easy recognition of the markers in a single slide. The use of the cldn18/maspin double-staining strategy in our study confirmed that these markers are useful in differentiating neoplasms from non-neoplastic epithelia in surgical specimens from the biliary tract.

In conclusion, we show that immunohistochemical staining cldn18, maspin, and p53 as a panel achieves reliable distinction of biliary tract cancers and BilINs from non-neoplastic epithelia in both surgical and biopsy specimens. This panel can serve to improve diagnostic accuracy and might aid the early diagnosis of biliary tract carcinoma and BilIN in presurgical biopsy specimens. This study is limited because it is retrospective; however, the high sensitivity and specificity observed suggests that this approach would support a diagnosis even in indeterminate cases. Further prospective and retrospective studies are needed to evaluate the practical value of this diagnostic method for clinical application.

Acknowledgments This work was supported by JSPS Grants-in-Aid for Scientific Research Grant Number 24790355.

Conflict of interest The authors declare that they have no conflict of interest.

References

1. Everhart JE, Ruhl CE (2009) Burden of digestive diseases in the United States Part III: liver, biliary tract, and pancreas. Gastroenterology 136: 1134–1144
2. Albores-Saavedra J, Schwartz AM, Batich K, Henson DE (2009) Cancers of the ampulla of vater: demographics, morphology, and survival based on 5,625 cases from the SEER program. J Surg Oncol 100:598–605
3. Matsuda A, Matsuda T, Shibata A et al (2013) Cancer incidence and incidence rates in Japan in 2007: a study of 21 population-based cancer registries for the Monitoring of Cancer Incidence in Japan (MCIJ) Project. Jpn J Clin Oncol 43:328–336
4. Nagakawa T, Kayahara M, Ikeda S et al (2002) Biliary tract cancer treatment: results from the Biliary Tract Cancer Statistics Registry in Japan. J Hepatobiliary Pancreat Surg 9:569–575
5. Ishihara S, Miyakawa S, Takada T et al (2007) Status of surgical treatment of biliary tract cancer. Dig Surg 24:131–136
6. Kawashima H, Itoh A, Ohno E, Goto H, Hirooka Y (2012) Transpapillary biliary forceps biopsy to distinguish benign biliary stricture from malignancy: how many tissue samples should be obtained? Dig Endosc 24(Suppl 1):22–27
7. Tamada K, Tomiyama T, Wada S et al (2002) Endoscopic transpapillary bile duct biopsy with the combination of intraductal ultrasonography in the diagnosis of biliary strictures. Gut 5:326–331
8. Mary L, Fan L, Haodong X, Deepti D, Besty OS, Hanlin LW (2010) S100P, von Hippel-Lindau gene product, and IMP3 serve as a useful immunohistochemical panel in the diagnosis of adenocarcinoma on endoscopic bile duct biopsy. Hum Pathol 41:1210–1219
9. Josse H, Meena P, Daniza M, Richard WC, Saverio L (2012) IMP3 immunocytochemical staining increases sensitivity in the routine cytologic evaluation of biliary brush specimens. Diagn Cytopathol 40:321–326
10. Kawashima H, Itoh A, Ohno E et al (2013) Diagnostic and prognostic value of immunohistochemical expression of S100P and IMP3 in transpapillary biliary forceps biopsy samples of extrahepatic bile duct carcinoma. J Hepatobiliary Pancreat Sci 20:441–447
11. Riener MO, Vogetseder A, Pestalozzi BC et al (2010) Cell adhesion molecules P-cadherin and CD24 are markers for carcinoma and dysplasia in the biliary tract. Hum Pathol 41:1558–1565
12. Tretiakova M, Antic T, Westerhoff M et al (2012) Diagnostic utility of CD10 in benign and malignant extrahepatic bile duct lesions. Am J Surg Pathol 36:101–108

13. Sato Y, Harada K, Sasaki M, Yasaka T, Nakanuma Y (2012) Heat shock proteins 27 and 70 are potential biliary markers for the detection of cholangiocarcinoma. Am J Pathol 180:123–130
14. Zen Y, Aishima S, Ajioka Y et al (2005) Proposal of histological criteria for intraepithelial atypical / proliferative biliary epithelial lesions of the bile duct inhepatolithiasis with respect to cholangiocarcinoma: preliminary report based on interobserver agreement. Pathol Int 55:180–188
15. Zen Y, Adsay NV, Bardadin K et al (2007) Biliary intraepithelial neoplasia: an international interobserver agreement study and proposal for diagnostic criteria. Mod Pathol 20:701–709
16. Nakamura Y, Curado MP, Franceschi S et al (2010) Intrahepatic cholangiocarcinoma. In: Bosman FT, Carneiro F, Hruban RH, Theise ND (eds) WHO classification of tumours of the digestive system, 4th edn. International Agency for Research on Cancer, Lyon, pp 217–224
17. Hsu M, Sasaki M, Igarashi S, Sato Y, Nakanuma Y (2013) KRAS and GNAS mutations and p53 overexpression in biliary intraepithelial neoplasia and intrahepatic cholangiocarcinomas. Cancer 119:1669–1674
18. Sawada N (2013) Tight junction-related human diseases. Pathol Int 63:1–12
19. Tsukita S, Yamazaki Y, Katsuno T, Tamura A, Tsukita S (2008) Tight junction-based epithelial microenvironment and cell proliferation. Oncogene 27:6930–6938
20. Singh AB, Sharma A, Dhawan P (2010) Claudin family of proteins and cancer: an overview. J Oncol 2010:541957
21. Niimil T, Nagashima K, Ward JM et al (2001) Claudin-18, a novel downstream target gene for the T/EBP/NKX2.1 homeodomain transcription factor, encodes lung- and stomach-specific isoforms through alternative splicing. Mol Cell Biol 21:7380–7390
22. Matsuda Y, Semba S, Ueda J et al (2007) Gastric and intestinal claudin expression at the invasive front of gastric carcinoma. Cancer Sci 98: 1014–1019
23. Merikallio H, Pääkkö P, Harju T, Soini Y (2011) Claudins 10 and 18 are predominantly expressed in lung adenocarcinomas and in tumors of nonsmokers. Int J Clin Exp Pathol 4:667–673
24. Soini Y, Takasawa A, Eskelinen M et al (2012) Expression of claudins 7 and 18 in pancreatic ductal adenocarcinoma: association with features of differentiation. J Clin Pathol 65:431–436
25. Shinozaki A, Shibahara J, Noda N et al (2011) Claudin-18 in biliary neoplasms. Its significance in the classification of intrahepatic cholangiocarcinoma. Virchows Arch 459:73–80
26. Ito T, Kojima T, Yamaguchi H et al (2011) Transcriptional regulation of claudin-18 via specific protein kinase C signaling pathways and modification of DNA methylation in human pancreatic cancer cells. J Cell Biochem 112:1761–1772
27. Zou Z, Anisowicz A, Hendrix MJC et al (1994) Maspin, a serpin with tumor-suppressing activity in human mammary epithelial cells. Science 263:526–529
28. Khalkhali-Ellis Z (2006) Maspin: the new frontier. Clin Cancer Res 24:7279–7283
29. Bettstetter M, Woenckhaus M, Wild PJ et al (2005) Elevated nuclear maspin expression is associated with microsatellite instability and high tumour grade in colorectal cancer. J Pathol 205:606–614
30. Rose SL, Fitzgerald MP, White NO et al (2006) Epigenetic regulation of maspin expression in human ovarian carcinoma cells. Gynecol Oncol 102:319–324
31. Akiyama Y, Maesawa C, Ogasawara S, Terashima M, Masuda T (2003) Cell-type-specific repression of the maspin gene is disrupted frequently by demethylation at the promoter region in gastric intestinal metaplasia and cancer cells. Am J Pathol 163:1911–1919
32. Fujisawa K, Maesawa C, Sato R et al (2005) Epigenetic status and aberrant expression of the maspin gene in human hepato-biliary tract carcinomas. Lab Invest 85:214–224
33. Cao D, Zhang Q, Wu LSF et al (2007) Prognostic significance of maspin in pancreatic ductal adenocarcinoma: tissue microarray analysis of 223 surgically resected cases. Mod Pathol 20:570–578
34. Shi J, Liu H, Wang HL, Prichard JW, Lin F (2013) Diagnostic utility of von Hippel-Lindau gene product, maspin, IMP3, and S100P in adenocarcinoma of the gallbladder. Hum Pathol 44:503–511
35. Rashid A, Ueki T, Gao YT et al (2002) K-ras mutation, p53 overexpression, and microsatellite instability in biliary tract cancers: a population-based study in China. Clin Cancer Res 8:3156–3163
36. Khan SA, Thomas HC, Toledano MB, Cox IJ, Taylor-Robinson SD (2005) p53 mutations in human cholangiocarcinoma: a review. Liver Int 25:704–716

Surg Today
DOI 10.1007/s00595-015-1120-8

REVIEW ARTICLE

Trials of vaccines for pancreatic ductal adenocarcinoma: Is there any hope of an improved prognosis?

Toru Mizuguchi · Toshihiko Torigoe · Fukino Satomi · Hiroaki Shima · Goro Kutomi · Shigenori Ota · Masayuki Ishii · Hiroshi Hayashi · Sumiyo Asakura · Yoshihiko Hirohashi · Makoto Meguro · Yasutoshi Kimura · Toshihiko Nishidate · Kenji Okita · Masaho Ishino · Atsushi Miyamoto · Masamitsu Hatakenaka · Noriyuki Sato · Koichi Hirata

Received: 5 September 2014 / Accepted: 6 January 2015

Abstract Pancreatic tumors are chemoresistant and malignant, and there are very few therapeutic options for pancreatic cancer, as the disease is normally diagnosed at an advanced stage. Although attempts have been made to develop vaccine therapies for pancreatic cancer for a couple of decades, none of the resultant protocols or regimens have succeeded in improving the clinical outcomes of patients. We herein review vaccines tested within the past few years, including peptide, biological and multiple vaccines, and describe the three sets of criteria used to evaluate the therapeutic activity of vaccines in solid tumors.

Keywords Pancreatic cancer · Vaccine · Immunomodulation

Introduction

Pancreatic cancer is the fourth leading cause of cancer-related death in the United States [1–3] and the fifth most common cause of such deaths in Japan [4]. Although surgical resection is considered to be the only curative therapy for pancreatic cancer, only 20 % of patients have resectable disease at the time of diagnosis [5, 6]. In addition, advanced pancreatic cancer patients exhibit a median survival time (MST) of approximately six months and a 5-year overall survival rate of less than 5 %, despite efforts to manage the tumors with chemotherapy, radiotherapy and other treatments [3, 5–8].

In 1997, Burris et al. reported that gemcitabine monotherapy is superior to fluorouracil (5-FU) monotherapy for

T. Mizuguchi · F. Satomi · H. Shima · G. Kutomi · S. Ota · M. Ishii · M. Meguro · Y. Kimura · T. Nishidate · K. Okita · K. Hirata
Department of Surgery, Surgical Oncology, Sapporo Medical University, Sapporo, Hokkaido 060-8543, Japan

T. Mizuguchi (✉)
Department of Surgery, Surgical Oncology, Sapporo Medical University School of Medicine, S-1, W-16, Chuo-Ku, Sapporo, Hokkaido 060-8543, Japan
e-mail: tmizu@sapmed.ac.jp

T. Torigoe · Y. Hirohashi · N. Sato
Department of Pathology I, Sapporo Medical University, Sapporo, Hokkaido 060-8543, Japan

H. Hayashi
Department of TR Management, Hokkaido Organization for Translational Research, Hokkaido University, Sapporo, Hokkaido 060-8638, Japan

S. Asakura
Department of Public Health, Sapporo Medical University, Sapporo, Hokkaido 060-8543, Japan

M. Ishino
Department of Intellectual Property Management Office, Sapporo Medical University, Sapporo, Hokkaido 060-8543, Japan

A. Miyamoto
Department of Hospital Pharmacy, Sapporo Medical University, Sapporo, Hokkaido 060-8543, Japan

M. Hatakenaka
Department of Diagnostic Radiology, Sapporo Medical University, Sapporo, Hokkaido 060-8543, Japan

Published online: 05 February 2015